PROCEEDINGS A

royalsocietypublishing.org/journal/rspa

Research

Cite this article: Green CC, Mahenthiram A, Ward LA. 2025 Harmonic-measure distribution functions of multiply connected domains with various geometries. *Proc. R. Soc. A* **481**: 20240392.
https://doi.org/10.1098/rspa.2024.0392

Received: 24 May 2024
Accepted: 16 June 2025

Subject Areas:
applied mathematics

Keywords:
harmonic-measure distribution function, prime function, multiply connected planar domain, conformal map, Brownian motion

Author for correspondence:
Arunmaran Mahenthiram
e-mail: arunmaran@univ.jfn.ac.lk

THE ROYAL SOCIETY PUBLISHING

Harmonic-measure distribution functions of multiply connected domains with various geometries

Christopher C. Green[1], Arunmaran Mahenthiram[2] and Lesley A. Ward[3]

[1]Department of Mathematics, Statistics and Physics, Wichita State University, Wichita, KS 67260, USA
[2]Department of Mathematics and Statistics, University of Jaffna, Jaffna 40000, Sri Lanka
[3]UniSA STEM, University of South Australia, Mawson Lakes, Adelaide, South Australia 5095, Australia

CCG, 0000-0001-5181-4037; AM, 0000-0001-9899-1292

The harmonic-measure distribution functions, or h-functions, associated with several classes of planar multiply connected domains $\Omega \subset \mathbb{C}$ and basepoint $z_0 \in \Omega$ locations are the principal objects of consideration in this paper. The h-function with respect to Ω and z_0 encodes the probability that a particle undergoing Brownian motion in Ω first collides with the boundary $\partial\Omega$ within a certain distance from the basepoint z_0 where it was initially released. Recently, Green *et al.* (Green *et al.* 2022 *Proc. R. Soc. A* **478**, 20210832. (doi:10.1098/rspa.2021.0832)) derived the first explicit formulae for the h-functions of multiply connected symmetrical rectilinear slit domains. In this paper, we generalize and extend the h-function calculations in Green *et al.* by considering various types of planar domains—those whose boundaries consist of either rectilinear slits or circles—as well as different locations of the basepoint. Throughout, we make judicious use of the Schottky-Klein prime function and its associated theory to derive analytical formulae for the h-functions. Our examples yield solutions to instances of a variant of the conformal Skorokhod embedding problem.

1. Introduction

The harmonic-measure distribution function is an object arising in potential theory that is closely related to the concept of Brownian motion and is a means of describing the geometry of a domain. Mostly referred to simply as the h-function, it is defined with respect to a planar domain in the complex plane and some basepoint in this domain. Formally, given a domain Ω in the extended complex plane and some basepoint $z_0 \in \Omega$, the associated h-function is the right-continuous, increasing function $h : [0, \infty) \to [0, 1]$ defined by

$$h(r) = h_{\Omega,z_0}(r) := \omega_{hm}(z_0, \partial\Omega \cap \overline{B(z_0, r)}, \Omega),$$

where ω_{hm} refers to harmonic measure, $B(z_0, r) := \{z \in \mathbb{C} : |z - z_0| < r\}$ and $h(0) = 0$. That is, the value of $h(r)$ is the value of the harmonic measure of the portion $E_r := \partial\Omega \cap \overline{B(z_0, r)}$ of the boundary $\partial\Omega$ lying within a distance r of the basepoint z_0. See, for example, figure 2. Indeed, the value $h(r)$ is precisely the probability that a particle undergoing Brownian motion in the interior of Ω first exits the domain Ω at a point on the boundary $\partial\Omega$ lying within distance r from the particle's point of release at the basepoint z_0. To envision this scenario, it is convenient to refer to a *capture circle* $|z - z_0| = r$ of radius r centred at the basepoint z_0. See [1, fig. 1].

It is also important to recall that harmonic measure is a conformally invariant quantity; consequently, the theory we develop below makes use of conformal mapping to facilitate building h-functions in a bounded circular domain, which is conformally equivalent to Ω.

Kakutani [2] was the first to make the significant connection linking two-dimensional Brownian motion with harmonic functions and the Dirichlet problem in partial differential equations, and specifically with harmonic measure in the sense of Nevanlinna. Of most relevance to us is the situation where a Brownian particle is released from a basepoint z_0 in a finitely connected bounded or unbounded planar domain Ω whose boundary components are Jordan curves, and E is the union of finitely many arcs on $\partial\Omega$. In broad terms, it is shown in [2, theorem 1] that the probability of the first exit from Ω occurring through E is a bounded harmonic function of $z_0 \in \Omega$, whose boundary values coincide with the indicator function $\mathbb{1}_E$ almost everywhere; in other words, this harmonic function of z_0 solves the Dirichlet problem on Ω with boundary values $\mathbb{1}_E$.

The h-functions were first investigated in detail by Walden & Ward [3], a variant of them having originally appeared in Brannan & Hayman's problem collection [4, Problem 6.116] in a problem posed by Stephenson. Subsequently, h-functions have been constructed for many simply connected domains (see the survey article [5] as well as [6–9], and the references therein) but only recently have h-functions begun to be computed for multiply connected domains. Green *et al.* [1] were able to construct analytical formulae for h-functions in the model case of multiply connected domains whose boundaries consist of an even number of collinear slits of equal length lying on the real axis, symmetrically placed about the imaginary axis, and with the basepoint lying on the real axis to the left of the boundary components. Examples for one, two, four and eight boundary components were computed in [1, §c]. Their construction was facilitated by the function theory of the Schottky-Klein prime function [10,11], a special function which neatly encapsulates the geometry of a particular domain and has the same functional form regardless of the connectivity.

The main aim of the current paper is to capitalize threefold on the work of Green *et al.* [1] by computing h-functions for a variety of multiply connected domains: (1) with boundary components of equal or unequal size, (2) with boundary components consisting of collinear slits, of parallel non-collinear slits, or of circles, and (3) with basepoints located either to one side of all boundary components or between two of the boundary components.

All the h-functions computed below for multiply connected domains are new and appear in this paper for the first time: examples 4.2–4.6 with collinear slits, 4.8–4.12 with parallel non-collinear slits and 5.1–5.6 with circles. Examples 4.2 and 4.3 use the same domain as in [1, §c(ii)], but the basepoints are different. Examples 4.1 and 4.7 involve simply connected domains whose h-functions were already well understood (for example, the h-function for a slight variant of example 4.1 is given in [1, eqns. (1.2) and (5.26)]), but here a different conformal map is used. We include them here since it is most transparent to explain our method on these simpler examples, before applying it to the multiply connected domains that follow.

These generalizations presented several challenges, including the construction of several non-trivial conformal mappings and the derivation of suitable functions with discontinuous boundary data. A similar methodology to ours, in combination with Schwarz-Christoffel formulae [12], facilitates the construction of h-functions for certain doubly connected polygonal domains [13]. Green & Nasser [14] have also contributed to generalizing the results in [1] by recently conducting numerical work making use of boundary integral equation methods to compute h-functions in highly multiply connected rectilinear slit domains.

The theory of h-functions yields solutions to a variant of the much-studied Skorokhod embedding problem (SEP) from probability and Brownian motion; see [15–20] and the references therein. The SEP asks: 'Can a given probability measure μ be embedded in Brownian motion B_t?' The subproblem known as the conformal Skorokhod embedding problem (CSEP) asks: 'Given a centred probability distribution μ on $\mathbb{R}$ with finite variance, can a simply connected domain $\Omega \subset \mathbb{C}$ containing 0 be found whose exit time T embeds μ by projecting the stopped Brownian motion B_T onto the real axis?' As an example, consider the atomic measure $\mu = \frac{1}{2}\delta_{-1} + \frac{1}{2}\delta_1$ with point masses of mass 1/2 at each of the points -1 and 1 on the real axis. Let Ω be the infinite strip between the vertical lines $x=-1$ and $x=1$. Start the Brownian motion from 0, and for each Brownian path B_t, stop the motion at the point B_T (reached at the exit time $t=T$ for that path), where the path first hits the boundary of Ω. By symmetry, the probability of that first exit point B_T lying on the left-hand line $x=-1$ is 1/2, the same as for the right-hand line $x=1$. Projecting vertically onto the real axis yields our atomic measure μ. In this example, it is simple to devise a suitable domain Ω, but for a general measure μ that is not the case.

While in this paper we mainly focus on the *forwards* problem of computing the h-function of a given domain Ω with a given basepoint z_0, here we briefly highlight the *inverse* problem of finding a domain and a basepoint whose h-function $h_{\Omega,z_0}(r)$ coincides with a given function $f(r)$. This inverse problem can be seen as a variant of the CSEP, in which our measure μ is supported not on the whole real axis but on the positive real axis, and a vertical orthogonal projection $x+iy \mapsto x$ of the domain boundary (and also of the exit probability measure it carries) onto the real axis is replaced by circular projection $r\,\mathrm{e}^{\mathrm{i}\theta} \mapsto r$ onto the positive real axis. Given a measure μ supported on the positive real axis, its cumulative distribution function F_μ is the increasing right-continuous function given by $F_\mu(r) := \mu((0,r])$ for $r>0$. Conversely, each increasing right-continuous function F on the positive real axis gives rise to a unique Borel measure μ generated by $\mu((a,b]) = F(b) - F(a)$. Such functions $F(r)$ can often be shown to arise as h-functions. In particular, every example in this paper solves an instance of our inverse problem by exhibiting a domain and basepoint whose h-function coincides with a given function $F(r)$ which is the cumulative distribution function of a given measure μ.

In other words, every example in this paper (and those in previous publications giving calculations of h-functions) solves an instance of this variant of the CSEP.

Our paper has the following structure. Section 2 outlines the relevant special function theory used in our construction of the h-functions. In §3, we discuss the overarching procedure we have chosen to adopt to compute our h-functions. Sections 4 and 5 present the derivations of the h-functions associated with various multiply connected domains whose boundaries consist of slits or circles, for several basepoint locations. Section 6 has our concluding remarks.

Throughout this paper, we use the principal branch of the complex logarithm, so that the values of the imaginary part $\arg z = \operatorname{Im}\log z$ lie in $[-\pi,\pi)$.

For the h-functions $h = h_{\Omega,z_0} : (0,\infty) \to [0,1]$ treated here, the set $(0,\infty)$ of values of r divides naturally into the disjoint union of finitely many intervals $(0,r_1)$, $[r_1,r_2)$, $\ldots$, $[r_{n_1},r_n)$, $[r_n,\infty)$, such that the way the h-function depends on r is different on each interval. In particular, $h(r)$ is given by a different formula on each interval, yielding a piecewise-defined function. We call these intervals the *regimes* of the h-function, ordered from left to right, so the first is $(0,r_1)$, the second is (r_1,r_2)

and so on. The number $n+1$ of regimes, the transition values r_j, $j \in \{1, \ldots, n\}$, between regimes and the precise form of the dependence of $h(r)$ on r in each regime are all determined by the shapes and configuration of the boundary components of Ω, together with the location of the basepoint $z_0 \in \Omega$. Typically, a transition value r_j occurs when, as the radius r of the capture circle $|z - z_0| = r$ increases through $r = r_j$, the capture circle either begins to capture or finishes capturing a component or components of the boundary $\partial\Omega$. (In more general domains, transition values also occur at values of r for which the capture circle meets a point where $\partial\Omega$ is not smooth.)

When the capture circle is centred at a different basepoint z_0, as the radius r increases, the capture circle may encounter or leave the boundary components in a different order, and at different values $r = r_j$, leading to a different set of regimes. See examples 4.4 and 4.5, with the same domain Ω but different basepoints. The h-functions both have five regimes, but the transition values differ, since they encode the different distances from each basepoint to the endpoints -0.5, -0.4, 0.2 and 1 of the boundary components.

2. The prime function

To begin, we present some key definitions and results involving the Schottky-Klein prime function $\omega(\zeta, \alpha)$ (referred to henceforth as simply the *prime function*) associated with a bounded circular domain D_ζ. The reader is referred to Crowdy's monograph [11] and the references therein for a full development of the prime function, and its properties and applications. In the calculations described in this paper, we made extensive use of the MATLAB software package for the prime function, available at [21]; see also [22].

The prime function $\omega(\zeta, \alpha)$ is an analytic and single-valued function of ζ, for all $\zeta, \alpha \in D_\zeta$, and has a simple zero at $\zeta = \alpha$. In the simply connected case, the circular domain D_ζ is the open unit disc $\mathbb{D}$, and the prime function is the simple monomial $\omega(\zeta, \alpha) = \zeta - \alpha$ for $\zeta, \alpha \in \mathbb{D}$. This is the only prime function with such a simple form. In the doubly connected case, the circular domain $D_\zeta = \{\zeta \in \mathbb{C} : \rho < |\zeta| < 1\}$ is a concentric annulus. The prime function associated with D_ζ can be written explicitly as the infinite product

$$\omega(\zeta, \alpha) = -\frac{\alpha}{C^2} P\left(\frac{\zeta}{\alpha}, \rho\right), \tag{2.1}$$

where the P-function is defined as

$$P(\zeta, \rho) := (1 - \zeta) \prod_{n=1}^{\infty} (1 - \rho^{2n}\zeta)(1 - \rho^{2n}\zeta^{-1}) \tag{2.2}$$

for $\zeta \in D_\zeta$, and the constant $C := \prod_{n=1}^{\infty}(1 - \rho^{2n})$. For higher connectivity cases, the circular domain D_ζ is formed by deleting the appropriate number of closed discs from the unit disc $\mathbb{D}$, and the prime function $\omega(\zeta, \alpha)$ is given by a more complicated infinite product formula defined in terms of a Schottky group determined by the connectivity and geometry of D_ζ. The singly and doubly connected cases are special cases of this formula.

The P-function satisfies the following identities:

$$P(\rho^2\zeta, \rho) = -\frac{1}{\zeta} P(\zeta, \rho) \quad \text{and} \quad P\left(\frac{1}{\zeta}, \rho\right) = -\frac{1}{\zeta} P(\zeta, \rho). \tag{2.3}$$

The prime function for a domain D_ζ of arbitrary connectivity satisfies the identities

$$\omega(\zeta, \alpha) = -\omega(\alpha, \zeta) \quad \text{and} \quad \overline{\omega}\left(\frac{1}{\zeta}, \frac{1}{\alpha}\right) = -\frac{1}{\zeta\alpha}\omega(\zeta, \alpha), \tag{2.4}$$

where $\zeta, \alpha \in D_\zeta$ and the Schwarz conjugate $\overline{\omega}$ of ω are defined by $\overline{\omega}(\zeta, \alpha) := \overline{\omega(\overline{\zeta}, \overline{\alpha})}$.

Denote by $\theta_j(\zeta)$ the Möbius maps given by

$$\theta_j(\zeta) := \delta_j + \frac{q_j^2\zeta}{1-\overline{\delta_j}\zeta}, \quad j=1,\dots,N-1,$$

where δ_j and q_j are the centre and the radius, respectively, of the inner boundary circle C_j in the circular domain D_ζ. (Together with their inverses, these Möbius maps $\theta_j(\zeta)$ generate the Schottky group mentioned above.) Moreover, $\theta_j(\zeta) = 1/\overline{\zeta}$ for $\zeta \in C_j$.

The prime function has the following important property [11,23]:

$$\omega(\theta_j(\zeta),\alpha) = \gamma_j(\zeta,\alpha)\omega(\zeta,\alpha), \quad j=1,\dots,N-1, \tag{2.5}$$

where

$$\gamma_j(\zeta,\alpha) := \exp\left[-2\pi\mathrm{i}\left(v_j(\zeta) - v_j(\alpha) + \frac{\tau_{jj}}{2}\right)\right]\sqrt{\theta_j'(\zeta)},$$

$v_j(\zeta)$ denotes the *integrals of the first kind* in D_ζ [11, §2.5], and τ_{jj} denotes a diagonal entry of the period matrix for D_ζ [11, §2.4]. The $v_j(\zeta)$ can be found numerically using the MATLAB package `SKPrime` [21]. For $\tau \in C_j$, the integrals of the first kind satisfy the equations:

$$v_j(\tau) = \overline{v_j}\left(\frac{1}{\tau}\right) = \overline{v_j\left(\frac{1}{\overline{\tau}}\right)}, \quad j=1,\dots,N-1. \tag{2.6}$$

Also,

$$\frac{\omega(\theta_j(\zeta),\alpha_1)}{\omega(\theta_j(\zeta),\alpha_2)} = \exp[2\pi\mathrm{i}(v_j(\alpha_1) - v_j(\alpha_2))]\frac{\omega(\zeta,\alpha_1)}{\omega(\zeta,\alpha_2)}. \tag{2.7}$$

The following set of harmonic functions, $\sigma_j(\zeta,\overline{\zeta})$, $j=1,\dots,N-1$, will be useful. These functions are harmonic everywhere in D_ζ and have boundary values such that

$$\sigma_j(\zeta,\overline{\zeta}) = \begin{cases} 1 & \text{for } \zeta \in C_j; \\ 0 & \text{for } \zeta \in C_k,\ k \neq j; \\ 0 & \text{for } \zeta \in C_0. \end{cases} \tag{2.8}$$

These functions can be written down explicitly in terms of prime functions, as shown in [24]. The analytic extension of $\sigma_j(\zeta,\overline{\zeta})$ to D_ζ is denoted by $\widetilde{\sigma}_j(\zeta)$.

When $D_\zeta = \{\rho < |\zeta| < 1\}$, the functions $v_1(\zeta)$ and $\sigma_1(\zeta,\overline{\zeta})$ admit particularly simple forms:

$$v_1(\zeta) = \frac{1}{2\pi\mathrm{i}}\log\zeta \quad \text{and} \quad \sigma_1(\zeta,\overline{\zeta}) = \frac{\log|\zeta|}{\log\rho}. \tag{2.9}$$

3. Procedure for computing *h*-functions

Let us now explain how we compute the values of the h-functions of multiply connected domains Ω. Our procedure is carried out in §§ 4 and 5 for specific domains with various geometries, connectivities and locations of the basepoint. It is important to note that translations, reflections and rotations of Ω, together with the basepoint z_0, leave the h-function unchanged.

Consider a domain Ω in the z-plane, and fix a basepoint z_0 in Ω. Let d be the distance from z_0 to the closest boundary point of Ω. For the regime $0 < r < d$, we have $h(r) = 0$. For each fixed $r \geq d$, we find $h(r)$ by the following procedure. Let $E_r := \partial\Omega \cap \overline{B(z_0,r)}$ be the part of the boundary $\partial\Omega$ that lies within distance r of z_0. The value $h(r)$ at r of the h-function is the probability that a Brownian particle released from z_0 first exits Ω through E_r, rather than through $\partial\Omega \setminus E_r$. This number $h(r)$ is given by the value $u(z_0)$ at z_0 of the harmonic function $u(z)$ that solves the following Dirichlet problem in Ω:

$$(\Delta)_{\Omega,r} : \begin{cases} \Delta u = 0 & \text{in } \Omega; \\ u \equiv \mathbb{1}_{E_r} & \text{on } \partial\Omega. \end{cases} \tag{3.1}$$

Here, the prescribed boundary values of $u(z)$ are 1 on E_r and 0 on $\partial\Omega \setminus E_r$.

We exploit the conformal invariance of harmonic measure to solve this Dirichlet problem $(\Delta)_{\Omega,r}$, by first transplanting $(\Delta)_{\Omega,r}$ to a new and tractable Dirichlet problem $(\Delta)_{D_\zeta,r}$ on a bounded circular domain D_ζ that is conformally equivalent to our domain Ω, and then solving $(\Delta)_{D_\zeta,r}$ on D_ζ. Specifically, let $f : D_\zeta \to \Omega$ denote a conformal map from D_ζ onto Ω (see §3a). Then our new Dirichlet problem on D_ζ is

$$(\Delta)_{D_\zeta,r} : \begin{cases} \Delta v = 0 & \text{in } D_\zeta; \\ v \equiv \mathbb{1}_{f^{-1}(E_r)} & \text{on } \partial D_\zeta. \end{cases} \tag{3.2}$$

(To avoid confusion, it is worth noting explicitly that although we have used the seemingly parallel notation $(\Delta)_{\Omega,r}$ and $(\Delta)_{D_\zeta,r}$, in most cases, the subset $f^{-1}(E_r)$ of ∂D_ζ is not simply the set of all points in ∂D_ζ that lie within distance r of ζ_0.)

Let ζ_0 be the preimage in D_ζ of the basepoint z_0 in Ω. Then, by the conformal invariance of harmonic measure, the desired value $u(z_0)$ at z_0 of the solution u of $(\Delta)_{\Omega,r}$ is equal to the value $v(\zeta_0)$ at ζ_0 of the solution v of $(\Delta)_{D_\zeta,r}$, and so also the desired value $h(r)$ is given by $v(\zeta_0)$.

Now we come to the key idea. The boundary values in our Dirichlet problem $(\Delta)_{D_\zeta,r}$ on D_ζ have a very specific form: on each boundary circle C_j, the boundary values can be identically 1, or identically 0, or else C_j is divided into two arcs, where the boundary values are identically 1 on one arc and identically 0 on the other. It turns out that we can use what are called *Cayley-type maps* [11] to construct a potential function $W(\zeta)$ on D_ζ whose imaginary part has these boundary values.

We define a potential function $W(\zeta)$ given by the logarithm of an appropriate Cayley-type map, plus some other terms (analytic on D_ζ) determined by the desired boundary values on the boundary circles of D_ζ. The harmonic function $\operatorname{Im} W(\zeta)$ then solves our Dirichlet problem $(\Delta)_{D_\zeta,r}$ on D_ζ, and its value at the point ζ_0 yields the value $h(r)$ at our r of the h-function of our target domain Ω with respect to the basepoint z_0. Finally, carrying out the construction above for each value of $r > d$ yields the full h-function.

We note that for most of the h-functions computed in this paper, both the conformal map $f : D_\zeta \to \Omega$ and the Cayley-type maps are defined in terms of the relevant prime function. Also, when the set of regimes changes due to a change in basepoint, the conformal map f is not affected, but the Cayley-type maps and hence the potential function $W(\zeta)$ must be calculated anew.

In §3b, we explain the Cayley-type maps for regions Ω of different connectivities. In §3c, we summarize the construction of the desired potential function $W(\zeta)$ in terms of appropriate Cayley-type maps. Furthermore, in §3d, we explain the numerical simulation process that we used to cross-check all our h-function calculations.

(a) Conformal mapping

Consider a bounded circular domain D_ζ in the ζ-plane, with connectivity N, having the unit circle C_0 as its outer boundary and $N-1$ non-intersecting circles C_j of radius q_j centred at δ_j, where $j = 1, \ldots, N-1$, as its inner boundaries. The domain D_ζ is defined as the region interior to the unit circle C_0 but exterior to the other circles C_j. See figures 2, 3 and 7. Owing to the three real degrees of freedom asserted by the Riemann-Koebe mapping theorem, for the types of target domain Ω considered herein—all of which are up-down symmetric across the real axis—we may choose all the centres δ_j to be real so that D_ζ is also symmetric across the real axis.

Our conformal map $f(\zeta)$ transforming the circular domain D_ζ onto our target domain Ω is either a radial-slit map (§4a), a parallel-slit map (§4b) or a Möbius map (§5).

(b) Cayley-type maps

The potential function $W(\zeta)$ is defined in terms of a suitable Cayley-type map which transforms our circular domain D_ζ onto the lower half-plane with certain slits deleted. These slits lie on rays emanating from the origin. The Cayley-type map transforms the boundary components of D_ζ to these slits and to the real line. See [1, fig. 6].

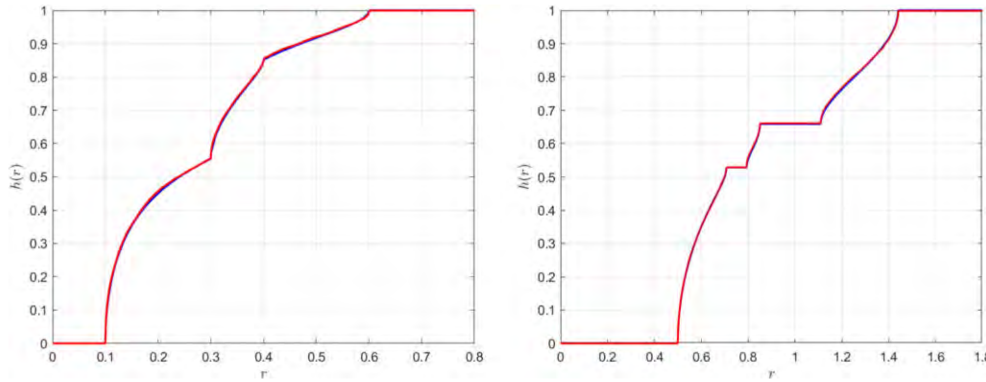

Figure 1. Superimposed calculated (blue) and simulated (red) h-function graphs for the doubly connected domain in example 4.3 (left) and for the triply connected domain in example 4.6 (right).

For simply connected regions Ω, our circular domain D_ζ is the open unit disc $\mathbb{D}$. Our Cayley-type map is simply the Möbius transformation known as the classical Cayley map; it maps the boundary of the unit disc onto the real line, and the interior of the disc onto the lower half-plane.

For multiply connected regions Ω, the Cayley-type map can be chosen so that it transforms any one boundary component of D_ζ onto the real line and transforms the others onto the above-mentioned slits in the lower half-plane. See [11, figs 5.8, 5.9, 6.10]. We choose which boundary component is to be mapped onto the real line depending on the location of the set $E_r = \partial\Omega \cap \overline{B(z_0, r)}$; this choice simplifies the construction of the potential function $W(\zeta)$ later. When E_r is contained in a single boundary component of Ω, we ensure that the corresponding boundary component of D_ζ (under the conformal map $f(\zeta)$) is the one mapped onto the real line. When E_r intersects two boundary components of Ω, we use a suitable *product* of Cayley-type maps either to transform one of the two corresponding boundary circles of D_ζ onto the real line or to transform both of them onto the real line, while simultaneously incorporating the required locations of the jump discontinuities. See discussion in example 4.2 around equation (4.8). Indeed, the usage of products of Cayley-type maps to construct the relevant potential functions for certain regimes of r is one of the main new technical points of this paper, and a deeper understanding of these products of Cayley-type maps is an ongoing matter of investigation.

(c) Potential functions

First, for each fixed r, by taking a logarithm of an appropriate Cayley-type map, piecewise constant values are assured on each boundary circle of D_ζ, with logarithmic singularities at the jump points corresponding to the zeroes and poles of the Cayley-type map. Second, the values of these constants can then be tweaked to be 1 or 0 as needed by adding certain extra summands. The imaginary part $v = \operatorname{Im} W(\zeta)$ of the resulting potential function $W(\zeta)$ on D_ζ solves our new Dirichlet problem $(\Delta)_{D_\zeta, r}$ on D_ζ. Evaluating $\operatorname{Im} W(\zeta)$ at ζ_0 yields the value of $h(r)$ at the chosen r.

We refer the reader to [11, §13.8] where the construction of a potential function by the approach we use here is worked through for a different problem, also with discontinuous boundary data.

(d) Numerical simulation

We used a numerical simulation of Brownian motion to cross-check the h-function formulae that we obtained via prime functions. Upon fixing a domain Ω and a basepoint $z_0 \in \Omega$, we simulate the release of millions of Brownian particles from z_0, and keep track of the exit locations where they first hit the boundary $\partial\Omega$. For each $r > 0$, the proportion of Brownian particles that hit $\partial\Omega$

within distance r of z_0 gives an approximate value for the number $h(r)$. In general, the higher the number of runs of the simulation, the more accurate this approximate value will be.

For every h-function reported in this paper, we carried out in MATLAB the numerical simulation process described above. In all cases, we obtained excellent agreement between the calculated and simulated h-functions. See figure 1, where for each of two specific domains, we plot the graphs of the theoretically calculated h-function and the numerically simulated h-function together on the same axes, for ease of comparison. For brevity, we omit the (similar) plots for the other h-functions calculated in this paper.

4. *h*-Functions for domains whose boundaries are slits

In this section, we compute the h-functions for domains Ω whose boundary components are either finitely many collinear slits (§4a) or finitely many non-collinear parallel slits whose midpoints lie on the real axis (§4b). We allow domains of different connectivity, and slits of equal or unequal lengths, as well as different locations of the basepoint z_0. To compute the h-functions of these domains, we first use appropriate conformal mappings such as the radial-slit mapping and the parallel-slit mapping to transform a bounded circular domain D_ζ onto our domain Ω, and then build an appropriate potential function on D_ζ.

(a) Radial-slit domains

The radial-slit conformal map

$$f(\zeta) = A\frac{\omega(\zeta,\alpha)\omega(\zeta,1/\overline{\alpha})}{\omega(\zeta,\beta)\omega(\zeta,1/\overline{\beta})}, \tag{4.1}$$

for $\alpha, \beta \in D_\zeta$, transforms a circular domain D_ζ onto a domain whose boundary components are slits which lie on rays emanating from the origin [11,25]. Here, A is a constant.

In §4a(i), we calculate the h-function for the complement of a single horizontal slit lying on the real axis, with a real basepoint z_0, highlighting the role of the prime function. In §4a(ii), we compute the h-functions for the complement of two collinear horizontal slits, with the basepoint z_0 located either to one side of both slits or between the slits. We consider slits of equal length (examples 4.2 and 4.3), and of unequal length (examples 4.4 and 4.5). The h-function computation for a domain with two equal-length collinear horizontal slits, when the basepoint z_0 is situated to the left of both slits, has already been described in [1]. In §4a(iii), we find the h-function for the triply connected domain whose boundary components are three unequal slits on the real axis, when the basepoint z_0 is fixed to the left of all three slits.

(i) Simply connected case

Example 4.1 (One slit with z_0 on the same line as the slit). When the target domain Ω is simply connected, the relevant circular domain is the unit disc $D_\zeta = \mathbb{D}$, with the unit circle $C_0 : |\zeta| = 1$ being the single boundary component. One can use elementary conformal maps from $\mathbb{D}$ to Ω. However, here we illustrate the use of the prime function to express a suitable conformal map from $\mathbb{D}$ to Ω, as a precursor to the higher connectivity cases treated below.

Consider the domain $\Omega = \mathbb{C}\backslash[-1, 1]$ with basepoint $z_0 = 2$. We use the radial-slit mapping

$$Q(\zeta) = A\frac{\omega(\zeta,\alpha)\omega(\zeta,1/\alpha)}{\omega(\zeta,\beta)\omega(\zeta,1/\beta)} = A\frac{(\zeta-\alpha)(\zeta-1/\alpha)}{(\zeta-\beta)(\zeta-1/\beta)}$$

from $D_\zeta = \mathbb{D}$ to the translated domain $\Omega' = \mathbb{C}\backslash[-3, -1]$ with basepoint $z_0' = 0$. Then the full conformal map from $D_\zeta = \mathbb{D}$ to Ω is $f(\zeta) = Q(\zeta) + 2$. The basepoint $z_0 = 2$ in Ω has preimage $\zeta_0 = f^{-1}(z_0)$ in Ω. We identify the constant A by enforcing the equation $Q(1) = -1$. We find the real parameters α and β by enforcing the remaining equations $Q(-1) = -3$ and $Q(\mathrm{i}) = -2 = Q(-\mathrm{i})$, and using multi-variable Newton iteration.

Next, we construct a suitable potential function on D_ζ, again illustrating the role of the prime function. Given an r in the regime $1 < r < 3$, the capture circle $|z - 2| = r$ encloses the part $E_r =$

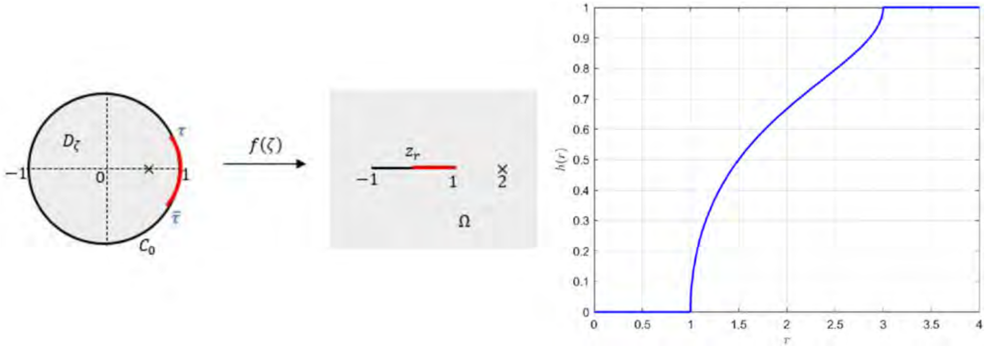

Figure 2. Conformal map $f(\zeta) = Q(\zeta) + 2$ from interior of unit disc to domain $\Omega = \mathbb{C}\backslash[-1, 1]$ with basepoint $z_0 = 2$ (left) and graph of $h(r)$ (right). The set E_r in Ω and its preimage in D_ζ are shown in red. Also, $z_r = f(\tau) = f(\overline{\tau})$ and $\tau = \mathrm{e}^{\mathrm{i}\phi}$ with $\mathrm{Im}\tau > 0$.

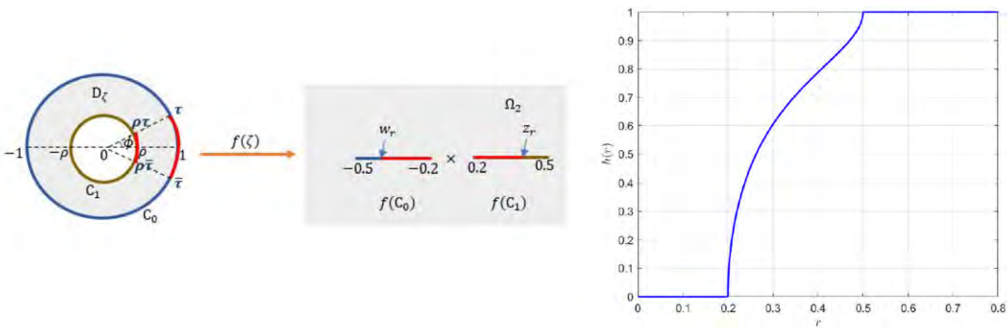

Figure 3. Conformal map $f(\zeta)$ from doubly connected concentric annulus D_ζ to an equal slit domain $\Omega_2 = \mathbb{C}\backslash([-0.5, -0.2] \cup [0.2, 0.5])$ with basepoint $z_0 = 0$, for the regime $0 \le r < 0.5$ (left) and graph of $h(r)$ (right). The set E_r in Ω_2 and its preimage in D_ζ are shown in red. Also, $w_r = f(\tau) = f(\overline{\tau})$ and $z_r = f(\rho\tau) = f(\rho\overline{\tau})$, and $\tau = \mathrm{e}^{\mathrm{i}\phi}$ with $\mathrm{Im}\tau > 0$.

$[z_r, 1]$ of the boundary $\partial\Omega$. Here, z_r denotes the point where the capture circle intersects $\partial\Omega$. Let $\tau = \mathrm{e}^{\mathrm{i}\phi}$ and $\overline{\tau} = \mathrm{e}^{-\mathrm{i}\phi}$ in ∂D_ζ, with $\phi > 0$, denote the preimages of z_r under the conformal map f. See the left-hand image in figure 2. We seek an analytic function W on D_ζ, whose imaginary part takes the value 1 on the set E_r (shown in red) and 0 on the set $\partial D_\zeta \setminus E_r$.

The classical Cayley map

$$R(\zeta, \tau, \overline{\tau}) = -\frac{1}{\tau}\frac{\omega(\zeta, \tau)}{\omega(\zeta, \overline{\tau})} = -\frac{1}{\tau}\frac{(\zeta - \tau)}{(\zeta - \overline{\tau})} \tag{4.2}$$

transforms the interior of the unit disc onto the lower half-plane, and maps the boundary of the disc onto the real axis. Define

$$W(\zeta, \tau, \overline{\tau}) = \frac{1}{\pi}(\log R(\zeta, \tau, \overline{\tau}) + \mathrm{i}\pi) = \frac{1}{\pi}\left(\log\left[-\frac{1}{\tau}\frac{(\zeta - \tau)}{(\zeta - \overline{\tau})}\right] + \mathrm{i}\pi\right). \tag{4.3}$$

Note how the term $\mathrm{i}\pi$ adjusts the boundary values of $\mathrm{Im}[W(\zeta, \tau, \overline{\tau})]$. For $\zeta \in C_0$, we obtain

$$\mathrm{Im}[W(\zeta, \tau, \overline{\tau})] = \begin{cases} \dfrac{1}{\pi}(0 + \pi) = 1 & \text{for } 0 \le |\arg\zeta| \le \phi \\ \dfrac{1}{\pi}(-\pi + \pi) = 0 & \text{for } \phi < |\arg\zeta| \le \pi \end{cases} = \mathbb{1}_{f^{-1}(E_r)}(\zeta). \tag{4.4}$$

Thus, the harmonic function ImW solves our Dirichlet problem $(\Delta)_{D_\zeta,r}$ in D_ζ, and so the composite map Im$W \circ f^{-1}$ solves our Dirichlet problem $(\Delta)_{\Omega,r}$ in the domain Ω. Hence,

$$h(r) = h_{\Omega,z_0}(r) = \mathrm{Im}[W(\zeta_0, \tau, \overline{\tau})], \quad \text{where } |f(\tau) - z_0| = r, \tag{4.5}$$

for each r in the regime $1 \le r < 3$. (We note that the function $W(\zeta, \tau, \overline{\tau})$ is different for each such r, since τ and $\overline{\tau}$ vary with r.) Also $h(r) = 0$ for the regime $0 \le r < 1$, and $h(r) = 1$ for the regime $r \ge 3$. The resulting h-function is plotted as a function of r in the right-hand image in figure 2.

Note that in (4.5), the h-function $h_{\Omega,z_0}(r)$ is given *implicitly* in terms of the radius r of the capture circle. The dependence is through $\tau = \mathrm{e}^{\mathrm{i}\phi}$ and $\overline{\tau} = \mathrm{e}^{-\mathrm{i}\phi}$, which depend on r through the conformal map $f : D_\zeta \to \Omega$, since by definition $f(\tau) = f(\overline{\tau}) = r$. However, for brevity, we write simply τ and ϕ instead of τ_r and ϕ_r. Similar remarks apply to the other examples below.

As a check of the above construction of the potential function, we note that a different method yields exactly the same h-function as in (4.5). Specifically, by the conformal invariance of Brownian motion, and by its symmetry in the disc, we can read off the harmonic measure at z_0 of E_r in Ω simply as the normalized angle of sight subtended at 0 by the arc $f^{-1}(E_r)$ in the disc $D_\zeta = \mathbb{D}$. We omit the details.

(ii) Doubly connected case

In this section, we compute the h-functions of doubly connected domains where the boundary consists of two real collinear slits of equal or unequal lengths, and where the basepoint z_0 is either between the slits or to the left (or right) of both slits. For the doubly connected case, the preimage of a bounded circular domain is a concentric annulus $D_\zeta = \{\zeta \in \mathbb{C} : \rho < |\zeta| < 1\}$.

First, we treat the symmetric case when the slits are of equal length, and the basepoint z_0 lies between the two slits, either exactly midway between them (example 4.2) or off-centre (example 4.3). The h-function computation for equal-length slits when the basepoint is fixed to the left (or right) of both slits was carried out in [1]. Second, we treat the asymmetric case when the two slits have different lengths, with basepoint either somewhere between them (example 4.4) or to the left of both slits (example 4.5).

Example 4.2 (Two equal collinear slits with z_0 midway between them). Consider the domain $\Omega_2 = \mathbb{C}\backslash([-0.5, -0.2] \cup [0.2, 0.5])$ with the basepoint $z_0 = 0$. The h-function of this domain with this basepoint is shown in the right-hand image of figure 3.

The boundary $\partial\Omega_2$ of the domain Ω_2 consists of two equal-length collinear slits on the real axis, symmetrically placed about the imaginary axis. Writing the radial-slit mapping (4.1) in terms of the P-function, we have

$$f(\zeta) = A\frac{P(\zeta/\alpha, \rho)P(\zeta\overline{\alpha}, \rho)}{P(\zeta/\beta, \rho)P(\zeta\overline{\beta}, \rho)}. \tag{4.6}$$

Since the real slits on the boundary $\partial\Omega_2$ are symmetrically placed about the imaginary axis, the parameters α and β are both real and such that $\alpha = -\beta = \sqrt{\rho}$. In addition, $f(\sqrt{\rho}) = 0$ and $f(-\sqrt{\rho}) = \infty$, and we fix $f(-1) = -0.5$, $f(1) = -0.2$, $f(\rho) = 0.2$ and $f(-\rho) = 0.5$. By using $f(-1) = -0.5$, we identify the constant A. It then follows that the conformal mapping

$$f(\zeta) = -\frac{P(1/\sqrt{\rho}, \rho)P(\sqrt{\rho}, \rho)}{2P(-1/\sqrt{\rho}, \rho)P(-\sqrt{\rho}, \rho)}\left[\frac{P(\zeta/\sqrt{\rho}, \rho)P(\zeta\sqrt{\rho}, \rho)}{P(-\zeta/\sqrt{\rho}, \rho)P(-\zeta\sqrt{\rho}, \rho)}\right] \tag{4.7}$$

transplants the concentric annulus D_ζ onto the symmetrical slit domain Ω_2. See the left-hand image of figure 3. Here, the boundary circles $C_0 : |\zeta| = 1$ and $C_1 : |\zeta| = \rho$ are mapped onto the intervals $[-0.5, -0.2]$ and $[0.2, 0.5]$, respectively. Also, the circle centred at zero with radius $\sqrt{\rho}$ is mapped onto the imaginary axis under the map f. We have $\zeta_0 = f^{-1}(z_0) = \sqrt{\rho} \in D_\zeta$ since $f(\zeta_0) = z_0 = 0 \in \Omega_2$. Note that we use similar notation z_r, w_r, τ, $\overline{\tau}$, ϕ and so on, in the examples below. For brevity, we omit this notation from the figure captions from here on.

To determine the h-function, we first consider the following product of two Cayley-type maps:

$$T(\zeta,\tau,\overline{\tau}) = A_0 \frac{P(\zeta/\tau,\rho)P(\zeta/(\rho\overline{\tau}),\rho)}{P(\zeta/\overline{\tau},\rho)P(\zeta/(\rho\tau),\rho)}, \tag{4.8}$$

and identify the prefactor A_0 by mapping both boundary circles $|\zeta|=1$ and $|\zeta|=\rho$ to the real axis. Here, we have two boundary components, C_0 and C_1, on which we want the imaginary part of the potential to be piecewise constant, taking values 0 and 1. We are applying the guiding principle noted in §3b: the Cayley-type map should be chosen so that it maps both these components to the real line, with the points τ, $\overline{\tau}$, σ and $\overline{\sigma}$ where the jumps occur being mapped to 0, ∞, 0 and ∞, respectively. Then the argument function (the imaginary part of the logarithm) applied to the lower half-plane will be piecewise constant on the correct parts of the real line; later on, we adjust its values on these parts to match those we want. In this example, the map T above, a product of Cayley-type maps, has the desired mapping properties on C_0 and C_1. We label $w_r = f(\tau) = f(\overline{\tau})$ and $z_r = f(\rho\tau) = f(\rho\overline{\tau})$, where $\tau = \mathrm{e}^{\mathrm{i}\phi}$ with $\mathrm{Im}\,\tau > 0$. By using the identities (2.3) of the P-function, we obtain the functional relation

$$\overline{T(\zeta,\tau,\overline{\tau})} = \frac{\overline{A_0}}{A_0}\frac{\overline{\tau}}{\tau}T(\zeta,\tau,\overline{\tau}),$$

which holds on both $|\zeta|=1$ and $|\zeta|=\rho$. With $A_0\tau = c$, where c is a real constant, we have that $\mathrm{Im}\,T = 0$ on both $|\zeta|=1$ and $|\zeta|=\rho$. We pick $c=-1$, so that $A_0 = -1/\tau$. The product of Cayley-type maps in (4.8) is then given by

$$T(\zeta,\tau,\overline{\tau}) = -\frac{1}{\tau}\frac{P(\zeta/\tau,\rho)P(\zeta/(\rho\overline{\tau}),\rho)}{P(\zeta/\overline{\tau},\rho)P(\zeta/(\rho\tau),\rho)}. \tag{4.9}$$

Note that $\arg T$ is the same on both circles and is equal to $k\pi$, for some $k \in \mathbb{Z}$. By defining

$$W(\zeta,\tau,\overline{\tau}) = \frac{1}{\pi}(\log T(\zeta,\tau,\overline{\tau}) + \mathrm{i}\pi), \tag{4.10}$$

we obtain the h-function to be $h(r) = \mathrm{Im}[W(\zeta_0,\tau,\overline{\tau})]$ for the regime $0.2 \le r = |f(\tau) - z_0| < 0.5$.

Example 4.3 (Two equal collinear slits with z_0 off-centre between them). Consider the same domain $\Omega_2 = \mathbb{C}\backslash([-0.5,-0.2]\cup[0.2,0.5])$, but now with the basepoint fixed off-centre between the slits at $z_0 = 0.1 \in \Omega_2$. The lower right image of figure 4 shows the graph of the h-function for this domain with this basepoint z_0. There is no change in the value of ρ obtained in example 4.2 nor the conformal map f given in (4.7). However, there is now a new second regime (figure 4a) for which the capture circle covers part of the right-most slit on the boundary $\partial\Omega_2$ but none of the left-most slit, as well as a new fourth regime (figure 4c) where the capture circle covers all of the right-most slit and only part of the left-most slit. Figure 4a–c illustrates the subset E_r (shown in red) for the three regimes of r where $h(r)$ is non-constant, for the domain Ω_2 with this off-centre basepoint z_0.

For the regime $0.1 \le r < 0.3$, the capture circle covers part of the right-most slit in Ω_2, and $f(\sigma) = z_r = f(\overline{\sigma})$, where $\sigma = \rho\,\mathrm{e}^{\mathrm{i}\phi}$. See figure 4a. In this case, we take the Cayley-type map

$$S_1(\zeta,\sigma,\overline{\sigma}) = \sigma\frac{P(\zeta/\sigma,\rho)}{P(\zeta/\overline{\sigma},\rho)}. \tag{4.11}$$

This map transforms the inner circle C_1 onto the real axis, and maps the outer circle C_0 onto a slit lying on a ray in the lower half-plane which emanates from the origin [11]. Since S_1 is real for $|\zeta|=\rho$, we have $\arg S_1 = k\pi$ on C_1, for some $k\in\mathbb{Z}$. For $|\zeta|=1$, we can show that

$$\frac{S_1(\zeta,\sigma,\overline{\sigma})}{\overline{S_1(\zeta,\sigma,\overline{\sigma})}} = \frac{\overline{\sigma}}{\sigma} = \mathrm{e}^{\mathrm{i}(-2\phi+2m\pi)}, \quad m\in\mathbb{Z}.$$

This gives $\arg S_1 = m\pi - \phi$ on C_0, where $m\in\mathbb{Z}$. Now, by defining the function

$$W_1(\zeta,\sigma,\overline{\sigma}) = -\frac{1}{\pi}\left(\log S_1(\zeta,\sigma,\overline{\sigma}) - \mathrm{i}\phi\frac{\log\zeta}{\log\rho} + \mathrm{i}\phi\right), \tag{4.12}$$

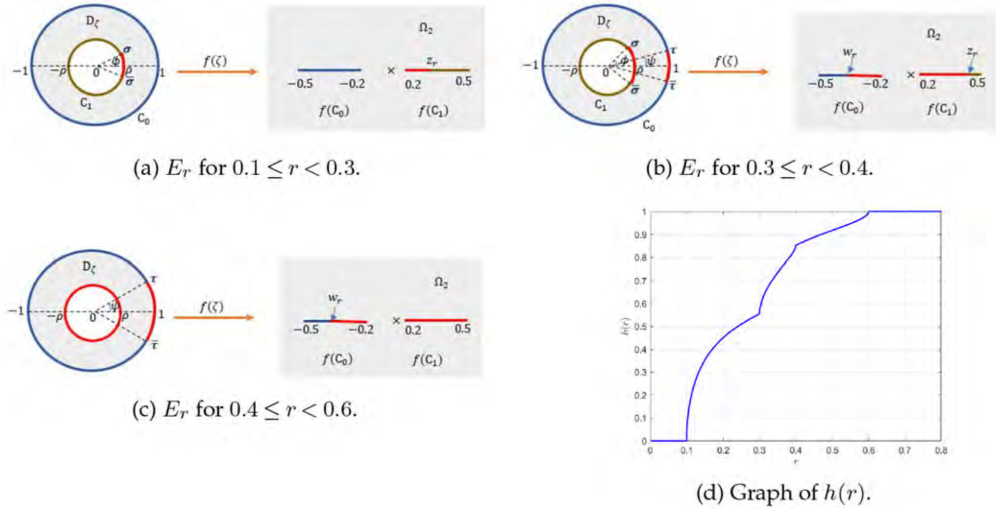

(a) E_r for $0.1 \le r < 0.3$.

(b) E_r for $0.3 \le r < 0.4$.

(c) E_r for $0.4 \le r < 0.6$.

(d) Graph of $h(r)$.

Figure 4. Conformal map from the doubly connected concentric annulus D_ζ to an equal slit domain $\Omega_2 = \mathbb{C}\backslash([-0.5, -0.2] \cup [0.2, 0.5])$ with basepoint $z_0 = 0.1$, for three regimes of r (top left, top right and lower left) and graph of $h(r)$ (lower right). The set E_r and its preimage are shown in red.

the harmonic function $\mathrm{Im}[W_1(\zeta_0, \sigma, \overline{\sigma})]$ gives the h-function for $0.1 \le r < 0.3$, where $\zeta_0 = f^{-1}(z_0)$.

Remark. We point out that the function $\widetilde{\sigma}_1(\zeta) = \log\zeta / \log\rho$ is the analytic extension of the harmonic function $\sigma_1(\zeta, \overline{\zeta})$ given in (2.9) and can also be expressed in terms of the single integral of the first kind as $\widetilde{\sigma}_1(\zeta) = 2\pi \mathrm{i} v_1(\zeta)/\log\rho$.

For the regime $0.3 \le r < 0.4$, the capture circle covers parts of both slits in Ω_2. Here, τ and $\overline{\tau}$ are the two preimage points of w_r, and σ and $\overline{\sigma}$ are the two preimage points of z_r, where $\tau = \mathrm{e}^{\mathrm{i}\psi}$ and $\sigma = \rho\, \mathrm{e}^{\mathrm{i}\phi}$ with $\phi > \psi$. See figure 4b. In this case, we define the following product of two Cayley-type maps

$$S(\zeta, \tau, \overline{\tau}, \sigma, \overline{\sigma}) = -\frac{1}{\sigma} \frac{P(\zeta/\tau, \rho) P(\zeta/\overline{\sigma}, \rho)}{P(\zeta/\overline{\tau}, \rho) P(\zeta/\sigma, \rho)}.$$

This function maps $C_1 : |\zeta| = \rho$ onto the real axis, so that $\arg S = k\pi$, for some $k \in \mathbb{Z}$. On $C_0 : |\zeta| = 1$, it can be shown that

$$\frac{S(\zeta, \tau, \overline{\tau}, \sigma, \overline{\sigma})}{\overline{S(\zeta, \tau, \overline{\tau}, \sigma, \overline{\sigma})}} = \frac{\overline{\tau}\sigma}{\tau\overline{\sigma}} = \mathrm{e}^{2ik_0\pi + 2\mathrm{i}(\phi - \psi)},\ k_0 \in \mathbb{Z}.$$

This gives $\arg S = k_0\pi + \phi - \psi$, $k_0 \in \mathbb{Z}$, on C_0. Now, by defining the function

$$W(\zeta, \tau, \overline{\tau}, \sigma, \overline{\sigma}) = \frac{1}{\pi}\left(\log S(\zeta, \tau, \overline{\tau}, \sigma, \overline{\sigma}) - \mathrm{i}(\psi - \phi)\frac{\log\zeta}{\log\rho} + \mathrm{i}(\pi + \psi - \phi)\right), \tag{4.13}$$

it follows that the harmonic function $\mathrm{Im}[W(\zeta_0, \tau, \overline{\tau}, \sigma, \overline{\sigma})]$ is the h-function for $0.3 \le r < 0.4$.

For the regime $0.4 \le r < 0.6$, the capture circle covers all of the right-most slit and part of the left-most slit in Ω_2. See figure 4c. In this case, we take

$$S_0(\zeta, \tau, \overline{\tau}) = -\tau \frac{P(\zeta/\tau, \rho)}{P(\zeta/\overline{\tau}, \rho)} \tag{4.14}$$

to be our Cayley-type map, with $\tau = \mathrm{e}^{\mathrm{i}\psi}$ [11]. This map transplants the circle C_0 onto the real axis and the circle C_1 onto a slit lying on a ray in the lower half-plane which emanates from the origin.

Then, $\mathrm{Im}S_0 = 0$ when $|\zeta| = 1$, and hence $\arg S_0 = k_0\pi$, $k_0 \in \mathbb{Z}$, on C_0. For $|\zeta| = \rho$, we can show that

$$\frac{S_0(\zeta,\tau,\overline{\tau})}{\overline{S_0(\zeta,\tau,\overline{\tau})}} = \frac{\tau}{\overline{\tau}} = \mathrm{e}^{\mathrm{i}(2\psi+2m\pi)},\ m \in \mathbb{Z}.$$

This gives $\arg S_0 = \psi + m\pi$ on C_1, where $m \in \mathbb{Z}$. Now, by defining the function

$$W_0(\zeta,\tau,\overline{\tau}) = \frac{1}{\pi}\left(\log S_0(\zeta,\tau,\overline{\tau}) - \mathrm{i}(\psi - \pi)\frac{\log\zeta}{\log\rho} + \mathrm{i}\pi\right), \tag{4.15}$$

we see that the h-function is given by the harmonic function $\mathrm{Im}[W_0(\zeta_0,\tau,\overline{\tau})]$ for $0.4 \le r < 0.6$.

In summary, the h-function $h(r) = h_{\Omega_2,0.1}(r)$ in this example is given by

$$h_{\Omega_2,0.1}(r) = \begin{cases} 0 & \text{if } 0 < r < 0.1; \\ \mathrm{Im}[W_1(\zeta_0,\sigma,\overline{\sigma})] & \text{if } 0.1 \le r < 0.3, \quad r = |f(\sigma) - z_0|; \\ \mathrm{Im}[W(\zeta_0,\tau,\overline{\tau},\sigma,\overline{\sigma})] & \text{if } 0.3 \le r < 0.4, \quad r = |f(\tau) - z_0| = |f(\sigma) - z_0|; \\ \mathrm{Im}[W_0(\zeta_0,\tau,\overline{\tau})] & \text{if } 0.4 \le r < 0.6, \quad r = |f(\tau) - z_0|; \\ 1 & \text{if } r \ge 0.6. \end{cases} \tag{4.16}$$

The implicit dependence of $h_{\Omega_2,0.1}(r)$ on r is through σ and τ.

We shall now turn our attention to h-functions for doubly connected slit domains when the symmetry condition is removed: the boundary intervals may now have *unequal* lengths. In this case, the condition $\alpha = -\beta = \sqrt{\rho}$ will no longer be valid.

Example 4.4 (Two unequal collinear slits with z_0 between them). Consider the domain $\Omega_2 = \mathbb{C}\backslash([-0.5,-0.4] \cup [0.2,1])$ whose boundary is two collinear slits of unequal length lying on the real axis. We use the radial-slit conformal map f, which transforms the concentric annulus D_ζ onto the domain Ω_2. The unit circle C_0 is mapped onto the slit $[-0.5,-0.4]$ while the inner circle C_1 is mapped onto the slit $[0.2,1]$. In addition, we require $f(-1) = -0.5$, $f(1) = -0.4$, $f(\rho) = 0.2$ and $f(-\rho) = 1$. To identify the constant A, we enforce $f(-1) = -0.5$; the three real parameters α, β, ρ are found by enforcing the other three equations via multi-variable Newton iteration. The conformal map f is now as follows:

$$f(\zeta) = -\frac{P(-1/\beta,\rho)P(-\beta,\rho)}{2P(-1/\alpha,\rho)P(-\alpha,\rho)}\left[\frac{P(\zeta/\alpha,\rho)P(\zeta\alpha,\rho)}{P(\zeta/\beta,\rho)P(\zeta\beta,\rho)}\right]. \tag{4.17}$$

We fix the basepoint $z_0 = -0.2 \in \Omega_2$ off-centre between the two slits. The graph of the h-function of the domain Ω_2 for this basepoint is shown in the right-hand image of figure 5. The subset E_r is the portion of the boundary $\partial\Omega_2$ that lies inside the capture circle of radius r centred at z_0. Let z_r be the point where the capture circle intersects the boundary $\partial\Omega_2$. The two preimages of z_r are τ and $\overline{\tau}$ on ∂D_ζ. The left-hand image of figure 5 illustrates the regime $0.4 \le r < 1.2$.

The h-function $h_{\Omega_2,-0.2}(r)$ is given by $\mathrm{Im}[W_0(\zeta_0,\tau,\overline{\tau})]$, $\mathrm{Im}[W_1(\zeta_0,\rho,\rho)]$ and $\mathrm{Im}[W_1(\zeta_0,\sigma,\overline{\sigma})]$ for the three regimes $0.2 \le r < 0.3$, $0.3 \le r < 0.4$ and $0.4 \le r < 1.2$, respectively, where $\tau = \mathrm{e}^{\mathrm{i}\psi}$, $\sigma = \rho\,\mathrm{e}^{\mathrm{i}\phi}$ and $\zeta_0 = f^{-1}(-0.2)$, and where the functions W_0 and W_1 are given by

$$W_0(\zeta,\tau,\overline{\tau}) = \frac{1}{\pi}\left(\log\left[-\tau\frac{P(\zeta/\tau,\rho)}{P(\zeta/\overline{\tau},\rho)}\right] - \mathrm{i}\psi\frac{\log\zeta}{\log\rho} + \mathrm{i}\pi\right) \tag{4.18}$$

and

$$W_1(\zeta,\sigma,\overline{\sigma}) = -\frac{1}{\pi}\left(\log\left[\sigma\frac{P(\zeta/\sigma,\rho)}{P(\zeta/\overline{\sigma},\rho)}\right] + \mathrm{i}(\pi - \phi)\frac{\log\zeta}{\log\rho} - \mathrm{i}(\pi - \phi)\right). \tag{4.19}$$

Note that the h-function is constant on the third regime $0.3 \le r < 0.4$, since for all r in this regime, the capture circle covers the entire left-most slit and none of the right-most slit. For these r, we have $h(r) = 1 - (\log|\zeta_0|/\log\rho)$, which is the value at $\zeta = \zeta_0$ of the unique harmonic function on D_ζ with boundary values 1 on C_0 and 0 on C_1; in other words, the solution to the Dirichlet problem $(\Delta)_{D_\zeta,r}$ with boundary values $\mathbb{1}_{C_1}(\zeta)$.

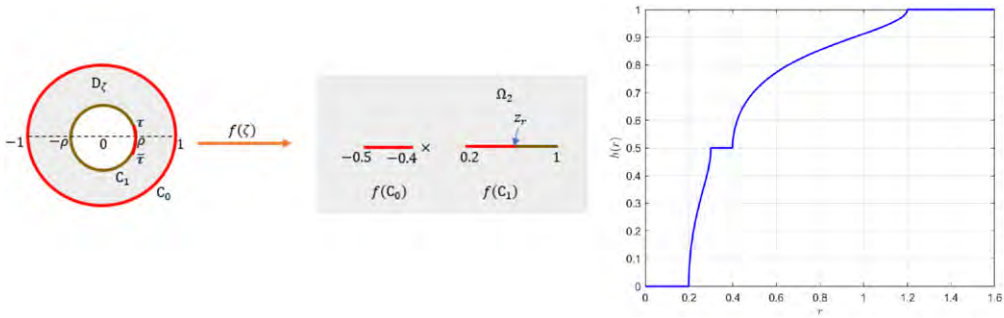

Figure 5. Conformal map from the doubly connected concentric annulus D_ζ to unequal slit domain $\Omega_2 = \mathbb{C}\backslash([-0.5, -0.4] \cup [0.2, 1])$ with basepoint $z_0 = -1$, for the regime $0.4 \leq r < 1.2$ (left) and graph of $h(r)$ (right). The set E_r and its preimage are shown in red. The step height of $h(r)$ is 0.5000.

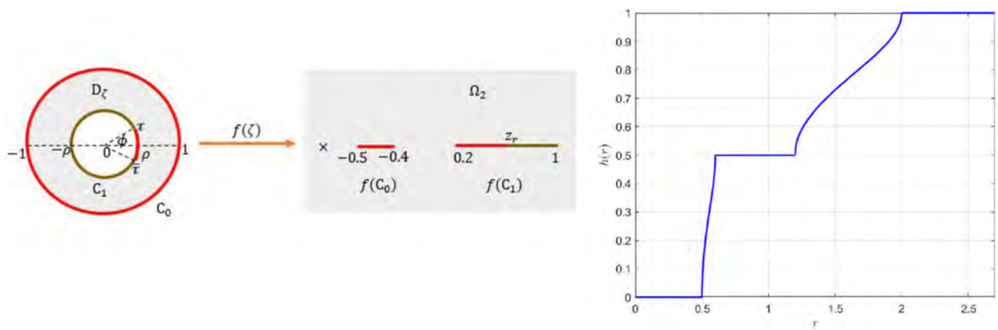

Figure 6. Conformal map from the doubly connected concentric annulus D_ζ to unequal slit domain $\Omega_2 = \mathbb{C}\backslash([-0.5, -0.4] \cup [0.2, 1])$ with basepoint $z_0 = -1$, for the regime $1.2 \leq r < 2$ (left) and graph of $h(r)$ (right). The set E_r and its preimage are shown in red. The step height of $h(r)$ is 0.5000.

In examples 4.2–4.4 above, the basepoint was located between the two collinear boundary slits. Next, we return to the situation treated in [1], where the basepoint is located to the left of both slits. However, we now allow the two slits to have unequal lengths. The calculations follow closely those in [1] and we suppress the details, indicating only where they differ.

Example 4.5 (Two unequal collinear slits with z_0 to their left). Consider the same domain $\Omega_2 = \mathbb{C}\backslash([-0.5, -0.4] \cup [0.2, 1])$ as in example 4.5. This time, we set the basepoint $z_0 = -1 \in \Omega_2$ to the left of both slits. The conformal map f remains as in (4.17).

The subset E_r is the part of the boundary $\partial\Omega_2$ which lies inside the capture circle of radius r centred at z_0. Let z_r be the point where the capture circle intersects the boundary $\partial\Omega_2$. The two preimages of this point are τ and $\overline{\tau}$ on ∂D_ζ. See the left-hand image of figure 6 which illustrates the regime $1.2 \leq r < 2$. The right-hand image of figure 6 shows the graph of $h(r)$ for the domain $\Omega_2 = \mathbb{C}\backslash([-0.5, -0.4] \cup [0.2, 1])$ with basepoint $z_0 = -1$.

In this case, the h-function $h_{\Omega_2,-1}(r)$ is given by $\mathrm{Im}[W_0(\zeta_0, \tau, \overline{\tau})]$, $1 - (\log|\zeta_0|/\log\rho)$ and $\mathrm{Im}[W_1(\zeta_0, \sigma, \overline{\sigma})]$ for the second, third and fourth regimes of r, respectively, with $\tau = \mathrm{e}^{\mathrm{i}\phi}$, $\sigma = \rho\mathrm{e}^{\mathrm{i}\phi}$ and $\zeta_0 = f^{-1}(-1)$, and where the function W_0 is defined by

$$W_0(\zeta, \tau, \overline{\tau}) = -\frac{1}{\pi}\left(\log\left[-\tau\frac{P(\zeta/\tau, \rho)}{P(\zeta/\overline{\tau}, \rho)}\right] - \mathrm{i}(\phi - \pi)\frac{\log\zeta}{\log\rho}\right), \tag{4.20}$$

and the function W_1 is as in (4.19).

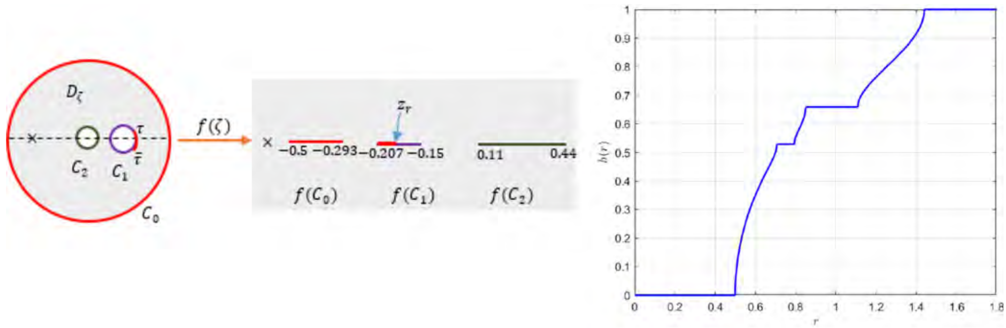

Figure 7. Conformal map from triply connected circular domain D_ζ to unequal slit domain $\Omega_3 = \mathbb{C}\backslash([-0.5, -0.293] \cup [-0.207, -0.15] \cup [0.11, 0.44])$ with basepoint $z_0 = -1$, for the regime $0.793 \leq r < 0.85$ (left) and graph of $h(r)$ (right). The set E_r and its preimage are shown in red. The step heights of $h(r)$ are 0.5285 and 0.6589.

(iii) Higher connectivity case

We turn to the calculation of the h-function of a triply connected domain whose boundary components are collinear unequal slits on the real axis, with the basepoint z_0 lying to the left of all three slits. Recall that in [1], h-functions were computed for domains consisting of an even number of equal-length slits. In example 4.6, where $N = 3$, we use the same formulae given in §§5a and 5b of [1] to compute the h-function.

Example 4.6 (Three unequal collinear slits with z_0 to their left). Consider the domain $\Omega_3 = \mathbb{C}\backslash([-0.5, -0.293] \cup [-0.207, -0.15] \cup [0.11, 0.44])$ with the basepoint $z_0 = -1 \in \Omega_3$ located to the left of all three slits. The corresponding triply connected circular domain D_ζ has three boundary circles C_0, C_1 and C_2, where the circle C_1 is centred at δ_1 with radius q_1 and the circle C_2 is centred at the origin with radius q_2. Let $\omega(\zeta, \cdot)$ be the prime function associated with D_ζ. The image of D_ζ under the radial-slit conformal map

$$f(\zeta) = A\frac{\omega(\zeta,\alpha)\omega(\zeta,1/\overline{\alpha})}{\omega(\zeta,\beta)\omega(\zeta,1/\overline{\beta})} \tag{4.21}$$

is the domain Ω_3. Since we have purely real slits, α and β are again real and lie inside the domain D_ζ. Under the mapping (4.21), the left-most and right-most slits in Ω_3 are the images of the circles C_0 and C_2, respectively, while the middle slit in Ω_3 is the image of C_1. Insisting that $f(-1) = -0.5$, $f(1) = -0.293$, $f(\delta_1 + q_1) = -0.207$, $f(\delta_1 - q_1) = -0.15$, $f(q_2) = 0.11$ and $f(-q_2) = 0.44$, we can identify the five parameters δ_1, q_1, q_2, α and β using multi-variable Newton iteration, along with the constant A via $f(-1) = 1$ and $\zeta_0 = f^{-1}(z_0)$. Figure 7 shows the action of the conformal map f on the triply connected circular domain D_ζ to produce the triply connected target domain Ω_3, along with the h-function.

(b) Parallel-slit domains

The parallel-slit conformal mapping

$$f_\theta(\zeta,\alpha) = \frac{1}{2\alpha} - \frac{1}{\omega(\zeta,\alpha)}\frac{\partial}{\partial\alpha}\omega(\zeta,\alpha) - \mathrm{e}^{2\mathrm{i}\theta}\left(\frac{1}{2\overline{\alpha}} + \frac{1}{\omega(\zeta,1/\overline{\alpha})}\frac{\partial}{\partial\overline{\alpha}}\omega(\zeta,1/\overline{\alpha})\right) \tag{4.22}$$

transforms a bounded circular domain D_ζ onto the complement of slits which are parallel to each other and are inclined at an angle θ to the positive real axis, while the point α is sent to infinity [25]. Equivalent formulae for $f_\theta(\zeta, \alpha)$ are given in [11].

In §4b(i), we determine the h-function of the domain $\Omega = \mathbb{C}\backslash[-1, 1]$ using a parallel-slit mapping. In §4b(ii), we compute the h-functions for some doubly connected domains whose boundary components are two vertical slits, with collinear midpoints and with either equal or

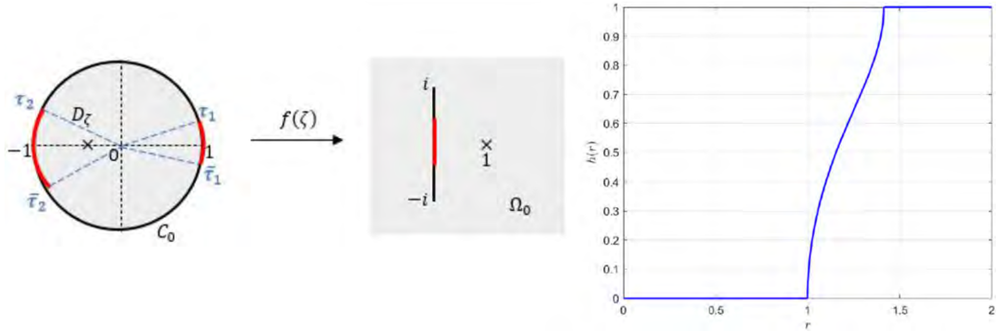

Figure 8. Conformal map from interior of unit disc to domain $\Omega_0 = \mathbb{C}\backslash[-\mathrm{i}, \mathrm{i}]$ with basepoint $z_0 = 1$, for the regime $1 \leq r < \sqrt{2}$ (left) and graph of $h(r)$ (right). The set E_r and its preimage are shown in red.

unequal lengths, where the basepoint z_0 is either between the slits or to the left (or right) of all the boundary slits. In §4b(iii), we carry out the computation of the h-function for a triply connected domain with unequal vertical slits when the basepoint z_0 is fixed on the real axis to the right of all the boundary slits.

(i) Simply connected case

Example 4.7 (One slit with z_0 on the bisector of the slit). The parallel-slit mapping for a single slit can be readily obtained from (4.22):

$$f_\theta(\zeta, \alpha) = \frac{1}{2\alpha} + \frac{1}{\zeta - \alpha} - \mathrm{e}^{2\mathrm{i}\theta}\left(\frac{1}{2\overline{\alpha}} + \frac{1}{\overline{\alpha}(\zeta\overline{\alpha} - 1)}\right). \tag{4.23}$$

As a check, let us first rederive the h-function for $\Omega = \mathbb{C}\backslash[-1, 1]$ with basepoint $z_0 = 2$ using (4.23) with $\theta = 0$. The conformal map $f(\zeta) = f_0(\zeta, \alpha)/2$ with $\alpha = 10^{-6}\mathrm{i}$ transforms the interior of the unit disc onto the complement of the interval $[-1, 1]$. Since $f(\zeta_0) = 2$, we have $\zeta_0 \approx 0.26795$. In this case, we of course have the same target domain as in figure 2; the only difference is the conformal map $f(\zeta)$, which in turn changes the relation between τ and r. Thus, by using the same functions $R(\zeta, \tau, \overline{\tau})$ and $W(\zeta, \tau, \overline{\tau})$ presented in §4a(i), we can express the h-function of the domain Ω via $\mathrm{Im}[W(\zeta_0, \tau, \overline{\tau})]$. We recover the same graph of the h-function as we obtained in figure 2, but now using $f(\zeta) = f_0(\zeta, \alpha)/2$.

Let us now derive the h-function for the domain $\Omega_0 = \mathbb{C}\backslash[-\mathrm{i}, \mathrm{i}]$ with basepoint $z_0 = 1$, using (4.23) with $\theta = \pi/2$. This time, the conformal map $f(\zeta) = -f_{\pi/2}(\zeta, \alpha)/2$ with $\alpha = 10^{-6}$ transforms the interior of the unit disc onto the domain Ω_0. Refer to the left-hand image of figure 8. The basepoint preimage is $\zeta_0 \approx -0.4142$. The h-function graph for the domain Ω_0 with basepoint $z_0 = 1$ is shown in the right-hand image of figure 8.

It is convenient here to use the following product of two classical Cayley maps

$$S_0(\zeta, \tau_1, \overline{\tau}_1, \tau_2, \overline{\tau}_2) = \frac{\tau_2}{\tau_1}\frac{(\zeta - \tau_1)(\zeta - \overline{\tau}_2)}{(\zeta - \overline{\tau}_1)(\zeta - \tau_2)}, \tag{4.24}$$

where $\tau_1 = \mathrm{e}^{\mathrm{i}\phi}$ and $\tau_2 = \mathrm{e}^{\mathrm{i}\psi}$, with $\psi > \phi$. Since S_0 is real on C_0, $\arg S = k\pi$, $k \in \mathbb{Z}$. By defining the function

$$W_0(\zeta, \tau_1, \overline{\tau}_1, \tau_2, \overline{\tau}_2) = \frac{1}{\pi}(\log S_0(\zeta, \tau_1, \overline{\tau}_1, \tau_2, \overline{\tau}_2) + \mathrm{i}\pi), \tag{4.25}$$

the harmonic function $\mathrm{Im}[W_0(\zeta_0, \tau_1, \overline{\tau}_1, \tau_2, \overline{\tau}_2)]$ gives the value of the h-function for $1 \leq r < \sqrt{2}$.

(ii) Doubly connected case

In this section, we compute the h-functions of doubly connected domains whose boundary components are two vertical slits whose midpoints lie on the real axis. The two slits can have

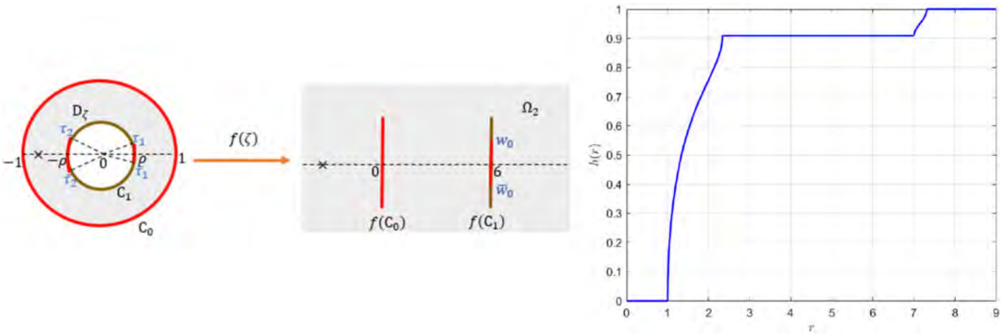

Figure 9. Conformal map from the doubly connected concentric annulus D_ζ to an equal parallel-slit domain Ω_2 with basepoint $z_0 = -1$, for the regime $7 \le r < 7.3115$ (left) and graph of $h(r)$ (right). The set E_r and its preimage are shown in red. The step height of $h(r)$ is 0.9090.

equal length or unequal length. The basepoint z_0 lies on the real axis, either to the left of both slits, midway between them or between them but off-centre. The appropriate preimage circular domain D_ζ is a concentric annulus $\rho < |\zeta| < 1$.

For doubly connected parallel-slit domains, the conformal mapping (4.22) can be rewritten as

$$f_\theta(\zeta,\alpha) = -\frac{1}{2\alpha} + \frac{1}{\alpha}K(\zeta/\alpha,\rho) + e^{2i\theta}\left(\frac{1}{2\overline{\alpha}} - \frac{1}{\overline{\alpha}}K(\zeta\overline{\alpha},\rho)\right), \tag{4.26}$$

where $K(\zeta/\alpha,\rho) = \zeta\,\partial(\log\omega(\zeta,\alpha))/\partial\zeta = \zeta\,\partial(\log P(\zeta/\alpha,\rho))/\partial\zeta$ [11, §5.12]. Since in our domains the boundary components are vertical slits, we have $\theta = \pi/2$ in (4.26). Therefore, the conformal mapping of D_ζ onto our target domains with two vertical slits is given by

$$f(\zeta) = f_{\pi/2}(\zeta,\alpha) = -\frac{1}{2\alpha} + \frac{1}{\alpha}K(\zeta/\alpha,\rho) - \frac{1}{2\overline{\alpha}} + \frac{1}{\overline{\alpha}}K(\zeta\overline{\alpha},\rho). \tag{4.27}$$

Example 4.8 (Two equal parallel slits with z_0 to their left). We fix the basepoint $z_0 = -1 \in \Omega_2$. Let us take a concentric annular domain $D_\zeta = \{\zeta \in \mathbb{C} : \rho < |\zeta| < 1\}$ with $\rho = f^{-1}(6)$ and fix $\alpha = -\sqrt{\rho}$ in (4.27). The conformal map $f(\zeta)$ in (4.27), when $\alpha = -\sqrt{\rho}$ with $\rho \approx 0.02778$, maps D_ζ onto the domain $\Omega_2 = \mathbb{C}\backslash([-2.1114i, 2.1114i] \cup [6 - 2.1114i, 6 + 2.1114i])$. The boundary circles C_0 and C_1 are mapped to the left-most and right-most vertical slits, respectively. The right-hand image in figure 9 shows the graph of the h-function of the domain Ω_2 with basepoint $z_0 = -1$.

In what follows, w_0 denotes a point in the boundary of Ω_2 where the capture circle of radius r centred at $z_0 = -1$ intersects one of the vertical slits, with $\operatorname{Im} w_0 \ge 0$. See figure 9. For the regime $1 \le r < 2.3362$, the capture circle covers part of the left-most slit and none of the right-most slit in $\partial\Omega_2$. In this case, the point $w_0 \in [0, 2.1114i)$ lies on the left-most slit and its preimage points lie on the outer boundary circle C_0 of D_ζ. Consider the following product of two Cayley-type maps

$$S_0(\zeta,\tau_1,\overline{\tau}_1,\tau_2,\overline{\tau}_2) = \frac{\tau_1}{\tau_2}\frac{P(\zeta/\tau_1,\rho)P(\zeta/\overline{\tau}_2,\rho)}{P(\zeta/\overline{\tau}_1,\rho)P(\zeta/\tau_2,\rho)}, \tag{4.28}$$

where $\tau_1 = e^{i\phi}$ and $\tau_2 = e^{i\psi}$, with $\psi > \phi$. For $|\zeta| = 1$, $\arg S_0 = k\pi$, $k \in \mathbb{Z}$, while for $|\zeta| = \rho$, $\arg S_0 = \phi - \psi + m\pi$, $m \in \mathbb{Z}$. Now, by defining the function

$$W_0(\zeta,\tau_1,\overline{\tau}_1,\tau_2,\overline{\tau}_2) = \frac{1}{\pi}\left(\log S_0(\zeta,\tau_1,\overline{\tau}_1,\tau_2,\overline{\tau}_2) - i(\pi + \phi - \psi)\frac{\log\zeta}{\log\rho} + i\pi\right), \tag{4.29}$$

we obtain the h-function $h(r) = \operatorname{Im}[W_0(\zeta_0,\tau_1,\overline{\tau}_1,\tau_2,\overline{\tau}_2)]$ for this regime of r, where $\zeta_0 = f^{-1}(-1)$.

For the regime $2.3362 \le r < 7$, the capture circle covers all of the left-most vertical slit, but none of the right-most vertical slit in Ω_2. It follows readily that the value of the h-function at our r is given by $h(r) = u(\zeta_0) \approx 0.9090$, where $u(\zeta) = 1 - (\log|\zeta|/\log\rho)$ is the unique harmonic function that solves the Dirichlet problem on D_ζ with boundary values 1 on C_0 and 0 on C_1.

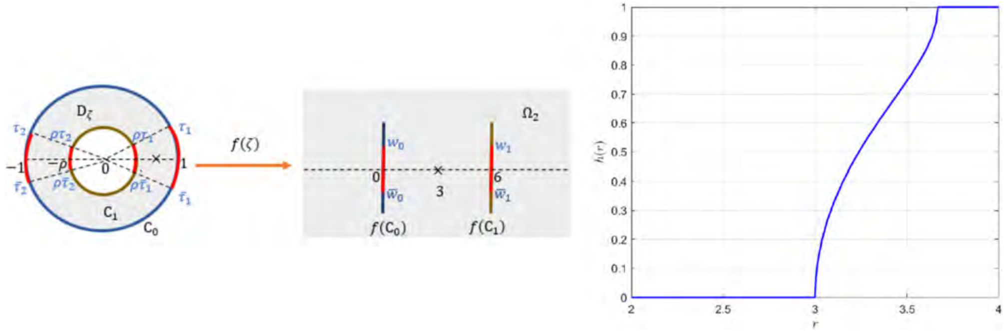

Figure 10. Conformal map from the doubly connected concentric annulus D_ζ to an equal parallel-slit domain Ω_2 with basepoint $z_0 = 3$, for the regime $3 \leq r < 3.6685$ (left) and graph of $h(r)$ (right). The set E_r and its preimage are shown in red.

For the regime $7 \leq r < 7.3115$, the capture circle covers all of the left-most slit and part of the right-most slit in Ω_2. Refer to the left-hand image in figure 9 which illustrates the conformal mapping for this regime. In this case, $w_0 \in [6, 6 + 2.1114\mathrm{i})$ is situated on the right-most slit in Ω_2. Also, the preimages under f of the points w_0 and $\overline{w}_0$ lie on the inner boundary circle C_1 of D_ζ. We define another product of Cayley-type maps

$$S_1(\zeta, \tau_1, \overline{\tau}_1, \tau_2, \overline{\tau}_2) = -\frac{\tau_1}{\tau_2} \frac{P(\zeta/\tau_1, \rho) P(\zeta/\overline{\tau_2}, \rho)}{P(\zeta/\overline{\tau_1}, \rho) P(\zeta/\tau_2, \rho)}, \tag{4.30}$$

where this time, $\tau_1 = \rho\, \mathrm{e}^{\mathrm{i}\phi}$ and $\tau_2 = \rho\, \mathrm{e}^{\mathrm{i}\psi}$, with $\psi > \phi$. For $|\zeta| = \rho$, we have that $\arg S_1 = k_0\pi$, $k_0 \in \mathbb{Z}$. For $|\zeta| = 1$, we can show that $\arg S_1 = -\phi + \psi + m_0\pi$, $m_0 \in \mathbb{Z}$. The h-function for this regime of r follows by defining the function

$$W_1(\zeta, \tau_1, \overline{\tau}_1, \tau_2, \overline{\tau}_2) = -\frac{1}{\pi}\left(\log S_1(\zeta, \tau_1, \overline{\tau}_1, \tau_2, \overline{\tau}_2) - \mathrm{i}(\phi - \psi)\frac{\log \zeta}{\log \rho} + \mathrm{i}(\phi - \psi)\right). \tag{4.31}$$

Example 4.9 (Two equal parallel slits with z_0 midway between them). We again consider the domain $\Omega_2 = \mathbb{C}\backslash([-2.1114\mathrm{i}, 2.1114\mathrm{i}] \cup [6 - 2.1114\mathrm{i}, 6 + 2.1114\mathrm{i}])$, but now take the basepoint $z_0 = 3 \in \Omega_2$. Then its preimage is $\zeta_0 = f^{-1}(z_0) = \sqrt{\rho} \in D_\zeta$. The h-function of this domain with basepoint $z_0 = 3$ is shown in the right-hand image of figure 10.

For the regime $3 \leq r < 3.6685$, the capture circle covers equal-length segments of both vertical slits in Ω_2. See figure 10. In this case, we define the following product of four Cayley-type maps:

$$S(\zeta, \tau_1, \overline{\tau}_1, \tau_2, \overline{\tau}_2) = \frac{\tau_2}{\tau_1} \frac{P(\zeta/\tau_1, \rho) P(\zeta/(\rho\overline{\tau}_1), \rho) P(\zeta/(\rho\tau_2), \rho) P(\zeta/\overline{\tau}_2, \rho)}{P(\zeta/\overline{\tau}_1, \rho) P(\zeta/(\rho\tau_1), \rho) P(\zeta/(\rho\overline{\tau}_2), \rho) P(\zeta/\tau_2, \rho)}, \tag{4.32}$$

where $\tau_1 = \mathrm{e}^{\mathrm{i}\phi}$ and $\tau_2 = \mathrm{e}^{\mathrm{i}\psi}$, with $\psi > \phi$. On both boundary circles of D_ζ, $\arg S = k\pi$, for some $k \in \mathbb{Z}$. Now, by defining the function

$$W(\zeta, \tau_1, \overline{\tau}_1, \tau_2, \overline{\tau}_2) = \frac{1}{\pi}(\log S(\zeta, \tau_1, \overline{\tau}_1, \tau_2, \overline{\tau}_2) + \mathrm{i}\pi), \tag{4.33}$$

the h-function in this regime is $h(r) = \mathrm{Im}[W(\zeta_0, \tau_1, \overline{\tau}_1, \tau_2, \overline{\tau}_2)]$ for this domain Ω_2 when the basepoint is fixed on the real axis, exactly midway between the slits.

Example 4.10 (Two equal parallel slits with z_0 off-centre between them). Consider the same domain $\Omega_2 = \mathbb{C}\backslash([-2.1114\mathrm{i}, 2.1114\mathrm{i}] \cup [6 - 2.1114\mathrm{i}, 6 + 2.1114\mathrm{i}])$ but with the basepoint z_0 fixed off-centre, at $z_0 = 2.8 \in \Omega_2$. See figure 11. From the parallel-slit mapping $f(\zeta)$ given in (4.27) and single-variable Newton iteration, we obtain the preimage ζ_0 of the basepoint z_0. Moreover, we have $\rho \approx 0.02778$, $\alpha = -\sqrt{\rho}$, $f(\rho) = f(-\rho) = 6$ and $f(1) = f(-1) = 0$.

royalsocietypublishing.org/journal/rspa Proc. R. Soc. A 481: 20240392

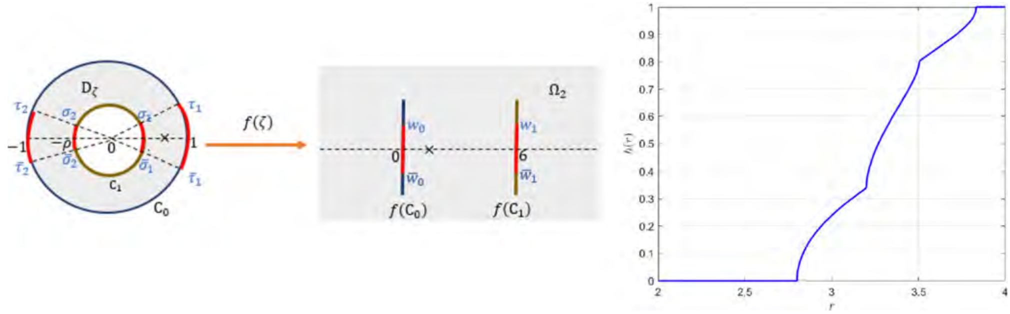

Figure 11. Conformal map from the doubly connected concentric annulus D_ζ to an equal parallel-slit domain Ω_2 with basepoint $z_0 = 2.8$, for the regime $3.2 \le r < 3.5069$ (left) and graph of $h(r)$ (right). The set E_r and its preimage are shown in red.

The left-hand image of figure 11 shows the subset E_r for the domain Ω_2 for the regime $3.2 \le r < 3.5069$ for this off-centre basepoint $z_0 = 2.8$, and the right-hand image shows the graph of the h-function.

The h-function $h_{\Omega_2,2.8}(r)$ is given by $\mathrm{Im}[W_0(\zeta, \tau_1, \overline{\tau}_1, \tau_2, \overline{\tau}_2)]$ for the regime $2.8 \le r < 3.2$, by $\mathrm{Im}[W(\zeta_0, \tau_1, \overline{\tau}_1, \tau_2, \overline{\tau}_2, \sigma_1, \overline{\sigma}_1, \sigma_2, \overline{\sigma}_2)]$ for the regime $3.2 \le r < 3.5069$ and by $\mathrm{Im}[W_1(\zeta_0, \sigma_1, \overline{\sigma}_1, \sigma_2, \overline{\sigma}_2)]$ for the regime $3.5069 \le r < 3.8338$. Here, the functions W_0 and W_1 are as in (4.29) and (4.31), respectively. In (4.29), the function S_0 is the same as in (4.28). Similarly, in (4.31), the function S_0 is the same as in (4.30). Also, the function W is given by

$$W = \frac{1}{\pi}\left(\log\left[\frac{1}{\sigma_1\overline{\sigma}_2}\frac{P(\zeta/\tau_1,\rho)P(\zeta/\overline{\tau}_2,\rho)P(\zeta/\overline{\sigma}_1,\rho)P(\zeta/\sigma_2,\rho)}{P(\zeta/\overline{\tau}_1,\rho)P(\zeta/\tau_2,\rho)P(\zeta/\sigma_1,\rho)P(\zeta/\overline{\sigma}_2,\rho)}\right]\right.$$
$$\left. + \mathrm{i}(\psi_0 - \phi_0 + \phi_1 - \psi_1)\frac{\log\zeta}{\log\rho} + \mathrm{i}(\pi + \phi_0 - \psi_0 - \phi_1 + \psi_1)\right).$$

Remark. The reader may wonder why we can use the same potential functions W_0 and W_1 for the same target domain with two different locations of the basepoint, as in examples 4.8 and 4.10, while still obtaining different h-functions. The explanation is that the potential functions are defined in terms of D_ζ and $f^{-1}(E_r)$, and both examples have the same form of circular domain D_ζ and subsets $f^{-1}(E_r)$ of ∂D_ζ. However, we have *different* conformal maps $f(\zeta)$ from D_ζ to Ω, and so the dependence of ζ_0, τ and σ on r is different in the two examples, leading to different h-functions $h(r)$ even though the potential functions are the same. Similar remarks apply to examples 4.3 and 5.3, where, in addition, the target domains have different geometry.

Example 4.11 (Two unequal parallel slits with z_0 to their left). In this example, we choose the same value of ρ as in examples 4.8, 4.9 and 4.10, but fix $\alpha = -0.1$ and the basepoint $z_0 = -1$. Now, the conformal map $f(\zeta)$ given in (4.27) transforms the concentric annulus D_ζ onto the new doubly connected domain $\Omega_2 = \mathbb{C}\backslash([-2.1737\mathrm{i}, 2.1737\mathrm{i}] \cup [10 - 6.0716\mathrm{i}, 10 + 6.0716\mathrm{i}])$, in which the vertical slits have unequal lengths. See figure 12. The calculation to compute the h-function is similar to that in example 4.8.

(iii) Higher connectivity case

Let us now turn to the construction of h-functions of higher connectivity domains whose boundary components are unequal vertical slits with midpoints on the real axis, when the basepoint z_0 is fixed on the real axis to the right (or left) of all boundary components.

The conformal mapping for a parallel-slit domain of connectivity greater than two is given in (4.22), where $\omega(\zeta, \cdot)$ is the prime function associated with the conformally equivalent multiply

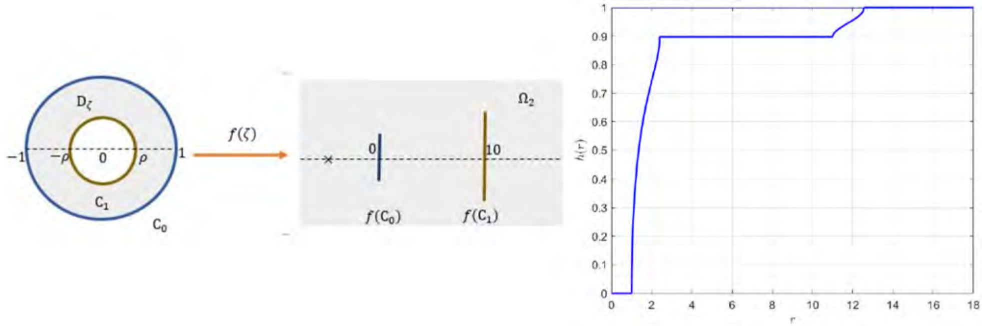

Figure 12. Conformal map from the doubly connected concentric annulus D_ζ onto unequal parallel-slit domain $\Omega_2 = \mathbb{C}\backslash([-2.1737\mathrm{i}, 2.1737\mathrm{i}] \cup [10 - 6.0716\mathrm{i}, 10 + 6.0716\mathrm{i}])$ (left) and graph of $h(r)$ (right) with basepoint $z_0 = -1$. The step height of $h(r)$ is 0.8978.

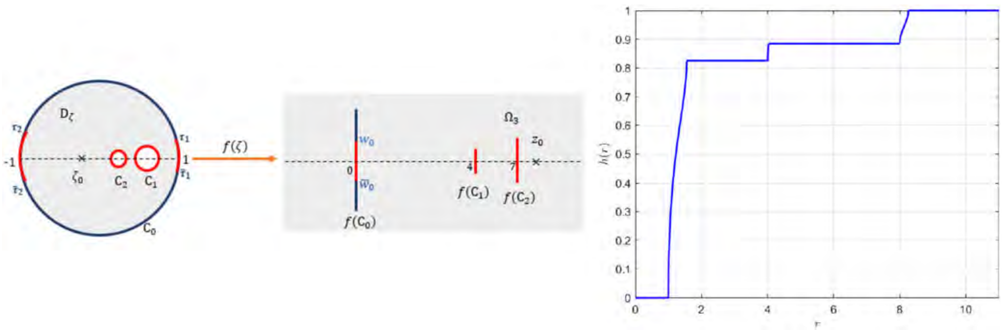

Figure 13. Conformal transformation from triply connected circular domain D_ζ to unequal parallel-slit domain Ω_3 with basepoint $z_0 = 8$, for the regime $8 \leq r < 8.2579$ (left) and graph of $h(r)$ (right). The set E_r and its preimage are shown in red. The step heights of $h(r)$ are 0.8252 and 0.8848.

connected circular domain D_ζ. When $\theta = \pi/2$, (4.22) becomes

$$f_{\pi/2}(\zeta, \alpha) = \frac{1}{2\alpha} - \frac{1}{\omega(\zeta, \alpha)} \frac{\partial}{\partial \alpha} \omega(\zeta, \alpha) + \frac{1}{2\overline{\alpha}} - \frac{1}{\omega(\zeta, 1/\overline{\alpha})} \frac{\partial}{\partial \overline{\alpha}} \omega(\zeta, 1/\overline{\alpha}). \tag{4.34}$$

Let us first present the derivation of the h-function for an unbounded N-connected domain Ω_N whose boundary components are N vertical slits with real midpoints, for an arbitrary finite $N > 0$, when the basepoint z_0 is real and fixed to the right of all N slits. For simplicity, we deal with domains in which the slits are far enough apart, compared to their lengths, that the capture circle of radius r centred at z_0 entirely covers each slit before covering any part of the next slit. Our methods also extend to treat domains without this property. The preimage domain D_ζ of Ω_N is an N-connected bounded circular domain D_ζ as in §3a, and we already have the conformal map f in (4.34) which transplants D_ζ onto Ω_N. Under f, the unit circle C_0 is mapped onto the left-most slit, while the circle C_{N-1} is mapped onto the right-most slit; the remaining slits lying in between are the images $f(C_1), \ldots, f(C_{N-2})$ labelled from left to right. The points 1 and -1 are mapped to the origin by the map f. See figure 13.

There are two cases to consider.

Case (I). For $\tau_m, \overline{\tau}_m \in C_0$, $m = 1, 2$, we consider the following product of two Cayley-type maps:

$$S_0(\zeta, \tau_1, \overline{\tau}_1, \tau_2, \overline{\tau}_2) = \frac{\tau_2}{\tau_1} \frac{\omega(\zeta, \tau_1)\omega(\zeta, \overline{\tau}_2)}{\omega(\zeta, \overline{\tau}_1)\omega(\zeta, \tau_2)},$$

which transforms the unit circle C_0 onto the real axis and sends the other $N-1$ boundary circles of D_ζ onto slits which lie on rays emanating from the origin in the lower half-plane. On C_0, we have that S_0 is real, so that $\arg S_0 = k_0\pi$, $k_0 \in \mathbb{Z}$. For $\zeta \in C_j, j=1,\ldots,N-1$, it can be shown that

$$e^{2\mathrm{i}\arg S_0(\zeta,\tau_1,\overline{\tau}_1,\tau_2,\overline{\tau}_2)} = \frac{S_0(\zeta,\tau_1,\overline{\tau}_1,\tau_2,\overline{\tau}_2)}{\overline{S_0(\zeta,\tau_1,\overline{\tau}_1,\tau_2,\overline{\tau}_2)}} = e^{2\pi\mathrm{i}[v_j(\tau_1)-v_j(\overline{\tau}_1)]}e^{-2\pi\mathrm{i}[v_j(\tau_2)-v_j(\overline{\tau}_2)]}.$$

Let

$$\widetilde{W}_0(\zeta,\tau_1,\overline{\tau}_1,\tau_2,\overline{\tau}_2) = \frac{1}{\pi}\log S_0(\zeta,\tau_1,\overline{\tau}_1,\tau_2,\overline{\tau}_2).$$

Now, the function $\mathrm{Im}[\widetilde{W}_0(\zeta,\tau_1,\overline{\tau}_1,\tau_2,\overline{\tau}_2)]$ has boundary values $\{0,-1\}$ on C_0. For brevity, here we use the short-hand notation $\{0,-1\}$ to mean that for $\zeta \in C_0$, with τ_1, τ_2 as in example 4.12 below,

$$\mathrm{Im}[\widetilde{W}_0(\zeta,\tau_1,\overline{\tau}_1,\tau_2,\overline{\tau}_2)] = \begin{cases} 0 & \text{for } |\arg\zeta| \le \arg\tau_1 \quad \text{and for } \arg\tau_2 < |\arg\zeta| \le \pi; \\ -1 & \text{for } \arg\tau_1 < |\arg\zeta| \le \arg\tau_2. \end{cases} \tag{4.35}$$

Adding 1, we obtain the desired boundary values $\{1,0\}$ on C_0:

$$\begin{aligned} 1+\mathrm{Im}[\widetilde{W}_0(\zeta,\tau_1,\overline{\tau}_1,\tau_2,\overline{\tau}_2)] &= 1+\frac{1}{\pi}\arg S_0(\zeta,\tau_1,\overline{\tau}_1,\tau_2,\overline{\tau}_2) \\ &= \begin{cases} 1+\{0,\frac{1}{\pi}(-\pi)\} = 1+\{0,-1\} = \{1,0\} & \text{for } \zeta \in C_0; \\ 1+[v_j(\tau_1)-v_j(\overline{\tau}_1)]-[v_j(\tau_2)-v_j(\overline{\tau}_2)] & \text{for } \zeta \in C_j,\ j=1,\ldots,N-1. \end{cases} \end{aligned} \tag{4.36}$$

It remains to adjust the boundary values on the other boundary circles C_j, while keeping the boundary values on C_0 unchanged. To do so, we will exploit the linearity of the Dirichlet problem by adding to the harmonic function in equation (4.36) additional terms involving the functions $\sigma_j(\zeta,\overline{\zeta})$, which are harmonic everywhere in D_ζ with boundary values as in equation (2.8).

Specifically, consider the potential function

$$W_0(\zeta,\tau_1,\overline{\tau}_1,\tau_2,\overline{\tau}_2) = \mathrm{i}+\widetilde{W}_0(\zeta,\tau_1,\overline{\tau}_1,\tau_2,\overline{\tau}_2)+\mathrm{i}\sum_{j=1}^{N-1}(-[v_j(\tau_1)-v_j(\overline{\tau}_1)]+[v_j(\tau_2)-v_j(\overline{\tau}_2)])\widetilde{\sigma}_j(\zeta), \tag{4.37}$$

where $\widetilde{\sigma}_j(\zeta)$ is the analytic extension to D_ζ of the harmonic function $\sigma_j(\zeta,\overline{\zeta})$. Then the function

$$\mathrm{Im}[W_0(\zeta,\tau_1,\overline{\tau}_1,\tau_2,\overline{\tau}_2)] = 1+\mathrm{Im}[\widetilde{W}_0(\zeta,\tau_1,\overline{\tau}_1,\tau_2,\overline{\tau}_2)]-\sum_{j=1}^{N-1}([v_j(\tau_1)-v_j(\overline{\tau}_1)]-[v_j(\tau_2)-v_j(\overline{\tau}_2)])\sigma_j(\zeta,\overline{\zeta}) \tag{4.38}$$

is harmonic and solves our Dirichlet problem $(\Delta)_{D_\zeta,r}$ in our circular domain D_ζ.

Case (II). For $\tau_m, \overline{\tau}_m \in C_k$, $k=1,\ldots,N-1$, $m=1,2$, we consider

$$\widetilde{W}_k(\zeta,\tau_1,\overline{\tau}_1,\tau_2,\overline{\tau}_2) = -\frac{1}{\pi}\log S_k(\zeta,\tau_1,\overline{\tau}_1,\tau_2,\overline{\tau}_2),$$

where

$$S_k(\zeta,\tau_1,\overline{\tau}_1,\tau_2,\overline{\tau}_2) = -\left(\frac{\tau_2-\delta_k}{\tau_1-\delta_k}\right)\frac{\omega(\zeta,\tau_1)\omega(\zeta,\overline{\tau}_2)}{\omega(\zeta,\overline{\tau}_1)\omega(\zeta,\tau_2)}$$

is a product of two Cayley-type maps that transplants the circle C_k onto the real axis and maps the other boundary circles onto slits lying on rays emanating from the origin in the lower half-plane.

For $\zeta \in C_0$,

$$e^{2\mathrm{i}\arg S_k(\zeta,\tau_1,\overline{\tau}_1,\tau_2,\overline{\tau}_2)} = \frac{S_k(\zeta,\tau_1,\overline{\tau}_1,\tau_2,\overline{\tau}_2)}{\overline{S_k(\zeta,\tau_1,\overline{\tau}_1,\tau_2,\overline{\tau}_2)}} = e^{-2\pi\mathrm{i}[v_k(\tau_1)-v_k(\overline{\tau}_1)]}\, e^{2\pi\mathrm{i}[v_k(\tau_2)-v_k(\overline{\tau}_2)]}.$$

For $\zeta \in C_k$, we have that S_k is real, so that $\arg S_k = k_1\pi$, $k_1 \in \mathbb{Z}$. For $\zeta \in C_j$, $j \neq k$, $j \neq 0$, it can be shown that

$$e^{2\mathrm{i}\arg S_k(\zeta,\tau_1,\overline{\tau}_1,\tau_2,\overline{\tau}_2)} = \frac{S_k(\zeta,\tau_1,\overline{\tau}_1,\tau_2,\overline{\tau}_2)}{\overline{S_k(\zeta,\tau_1,\overline{\tau}_1,\tau_2,\overline{\tau}_2)}} = e^{-2\pi\mathrm{i}[v_k(\tau_1)-v_k(\overline{\tau}_1)]} e^{2\pi\mathrm{i}[v_k(\tau_2)-v_k(\overline{\tau}_2)]} \cdot e^{2\pi\mathrm{i}[v_j(\tau_1)-v_j(\overline{\tau}_1)]} e^{-2\pi\mathrm{i}[v_j(\tau_2)-v_j(\overline{\tau}_2)]}.$$

Now, we see that the function $\mathrm{Im}[\widetilde{W}_k(\zeta,\tau_1,\overline{\tau}_1,\tau_2,\overline{\tau}_2)]$ has the desired boundary values $\{1,0\}$ on C_k. In particular,

$$\begin{aligned}\mathrm{Im}[\widetilde{W}_k(\zeta,\tau_1,\overline{\tau}_1,\tau_2,\overline{\tau}_2)] &= -\frac{1}{\pi}\arg S_k(\zeta,\tau_1,\overline{\tau}_1,\tau_2,\overline{\tau}_2)\\ &= \begin{cases} [v_k(\tau_1)-v_k(\overline{\tau}_1)] - [v_k(\tau_2)-v_k(\overline{\tau}_2)] & \text{for } \zeta \in C_0;\\ -\{\frac{1}{\pi}(-\pi),0\} = \{1,0\} & \text{for } \zeta \in C_k;\\ -[v_k(\tau_2)-v_k(\overline{\tau}_2)] + [v_k(\tau_1)-v_k(\overline{\tau}_1)] & \\ -[v_j(\tau_1)-v_j(\overline{\tau}_1)] + [v_j(\tau_2)-v_j(\overline{\tau}_2)] & \text{for } \zeta \in C_j, j<k, j\neq 0;\\ 1-[v_k(\tau_2)-v_k(\overline{\tau}_2)] + [v_k(\tau_1)-v_k(\overline{\tau}_1)] & \\ -[v_j(\tau_1)-v_j(\overline{\tau}_1)] + [v_j(\tau_2)-v_j(\overline{\tau}_2)] & \text{for } \zeta \in C_j,\ j>k,\ j\neq 0.\end{cases}\end{aligned} \tag{4.39}$$

It remains to adjust the boundary values on the other boundary circles C_0 and C_j, $j \neq k$, while keeping the boundary values on C_k unchanged. Again we add to the harmonic function in (4.39), appropriate additional terms involving the functions $\sigma_j(\zeta,\overline{\zeta})$. Let

$$\begin{aligned}W_k(\zeta,\tau_1,\overline{\tau}_1,\tau_2,\overline{\tau}_2) = \widetilde{W}_k(\zeta,\tau_1,\overline{\tau}_1,\tau_2,\overline{\tau}_2) - \mathrm{i}([v_k(\tau_1)-v_k(\overline{\tau}_1)] - [v_k(\tau_2)-v_k(\overline{\tau}_2)])(1-\widetilde{\sigma}_k(\zeta))\\ + \mathrm{i}\sum_{j\neq k,0}^{N-1}([v_j(\tau_1)-v_j(\overline{\tau}_1)] - [v_j(\tau_2)-v_j(\overline{\tau}_2)])\widetilde{\sigma}_j(\zeta).\end{aligned} \tag{4.40}$$

Finally,

$$\begin{aligned}\mathrm{Im}[W_k(\zeta,\tau_1,\overline{\tau}_1,\tau_2,\overline{\tau}_2)] = \mathrm{Im}[\widetilde{W}_k(\zeta,\tau_1,\overline{\tau}_1,\tau_2,\overline{\tau}_2)] - ([v_k(\tau_1)-v_k(\overline{\tau}_1)] - [v_k(\tau_2)-v_k(\overline{\tau}_2)])(1-\sigma_k(\zeta,\overline{\zeta}))\\ + \sum_{j\neq k,0}^{N-1}([v_j(\tau_1)-v_j(\overline{\tau}_1)] - [v_j(\tau_2)-v_j(\overline{\tau}_2)])\sigma_j(\zeta,\overline{\zeta})\end{aligned} \tag{4.41}$$

is harmonic and solves our Dirichlet problem $(\Delta)_{D_\zeta,r}$ in our circular domain D_ζ.

In our next example, we carry out the method above for a triply connected unequal parallel-slit domain Ω_3 when the basepoint z_0 is fixed to the right of all boundary slits of the domain Ω_3.

Example 4.12 (Three unequal vertical slits with z_0 to their right). Consider the domain Ω_3 whose boundary components are $[-2.0478\mathrm{i}, 2.0478\mathrm{i}]$, $[4-0.4392\mathrm{i}, 4+0.4392\mathrm{i}]$ and $[7-1.1851\mathrm{i}, 7+1.1851\mathrm{i}]$. The preimages of these vertical slits are the three boundary circles C_0, C_1 and C_2 of the circular domain D_ζ, where C_0 is the unit circle, and the circles C_1 and C_2 are centred at δ_1 and δ_2 with radii q_1 and q_2, respectively. See figure 13. Using the conformal map in (4.34), the five mapping parameters δ_1, δ_2, q_1, q_2 and α are found via multi-variable Newton iteration by enforcing the equations $f(1)=0=f(-1)$, $f(\delta_1+q_1)=4=f(\delta_1-q_1)$ and $f(\delta_2+q_2)=7=f(\delta_2-q_2)$.

We fix the basepoint $z_0 = 8 \in \Omega_3$. By using single-variable Newton iteration, we identify ζ_0, which satisfies the equation $\zeta_0 = f^{-1}(z_0)$. Figure 13 shows the subset E_r for the regime $8 \le r < 8.2579$, and the graph of $h(r)$ for this triply connected domain with $z_0 = 8$. Here, the points τ_1 and τ_2 are the preimages of w_0 under f, and similarly for their conjugates $\overline{\tau_1}$, $\overline{\tau_2}$ and $\overline{w_0}$.

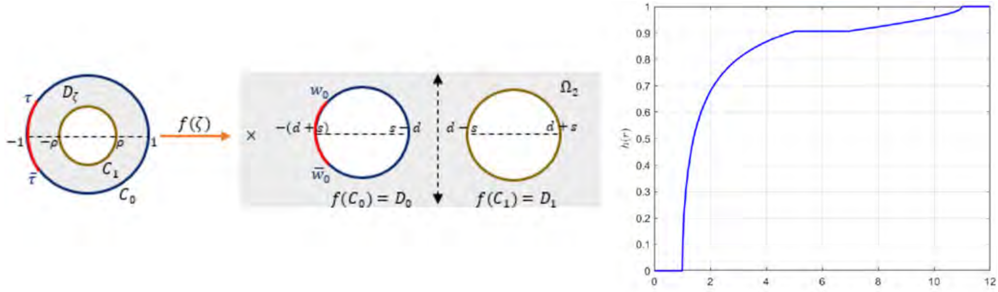

Figure 14. Conformal map from the doubly connected concentric annulus D_ζ to domain Ω_2 with equal discs with basepoint $z_0 = -k$, for the regime $k - (d+s) \leq r < k - (d-s)$ (left) and graph of $h(r)$ (right). The set E_r and its preimage are shown in red. The step height of $h(r)$ is 0.9068.

By using the MATLAB package `SKPrime` [21] for computing the prime function $\omega(\zeta, \alpha)$ in circular domains of higher connectivity, we can calculate the values of the integrals of the first kind $v_j(\zeta)$. We then apply the same formulae we obtained above for general connectivity N to compute the h-function of this domain. Here, the domain is triply connected, so $N = 3$.

5. h-Functions for domains whose boundaries are circles

In this section, we determine h-functions for domains whose boundary components are circles. The h-function for the exterior of a single disc is described in [3]. Here we consider h-functions for the exterior of two discs or of three discs, with collinear centres, with different locations of the basepoint z_0. We use a Möbius map f which transforms a bounded circular domain D_ζ onto the complement of the discs. In §5a, we compute the h-functions of doubly connected domains whose boundary components are two circles of equal size, or unequal size, for various locations of the basepoint z_0. In §5b, we calculate the h-function of a triply connected domain with three equal-sized discs, when the basepoint z_0 is fixed to the left (or right) of all three discs.

(a) Doubly connected case

Here, we compute the h-functions of the complement of two discs of equal or unequal size, when the basepoint z_0 is either to the left of, midway between, or off-centre between the discs.

Example 5.1 (Two equal discs with z_0 to their left). Consider the domain $\Omega_2 = \mathbb{C} \backslash (\{|z+d| \leq s\} \cup \{|z-d| \leq s\})$, where the two boundary circles have the same radius s but different centres $-d$, d, with $d > s > 0$. Place the basepoint z_0 on the real line to the left of both boundary circles, collinear with their centres. See figure 14. The following Möbius map f transforms the concentric annulus $D_\zeta = \{\zeta \in \mathbb{C} : \rho < |\zeta| < 1\}$ onto the domain Ω_2:

$$f(\zeta) = \sqrt{d^2 - s^2} \left(\frac{\sqrt{\rho} - \zeta}{\sqrt{\rho} + \zeta} \right). \tag{5.1}$$

Here, $\rho = ((\sqrt{d+s} - \sqrt{d-s})/(\sqrt{d+s} + \sqrt{d-s}))^2 < 1$ [26]. This Möbius map f transforms $C_0 : |\zeta| = 1$ onto the boundary circle $|z+d| = s$, and $C_1 : |\zeta| = \rho$ onto the boundary circle $|z-d| = s$. Also, let $\zeta_0 = f^{-1}(z_0) \in D_\zeta$, where $z_0 = -k < -(d+s) < 0$.

The left-hand image of figure 14 is drawn for the regime $k - (d+s) \leq r < k - (d-s)$. In this case, the capture circle covers part of the left-most boundary circle $|z+d| = s$. Here, $f(\tau) = w_0$, $f(\bar{\tau}) = \overline{w}_0$, $\tau = e^{i\phi}$ and $\mathrm{Im}\tau > 0$. The right-hand image of figure 14 shows the graph of the h-function for Ω_2 with $z_0 = -k = -6$, $d = 3$, $s = 2$.

royalsocietypublishing.org/journal/rspa Proc. R. Soc. A 481: 20240392

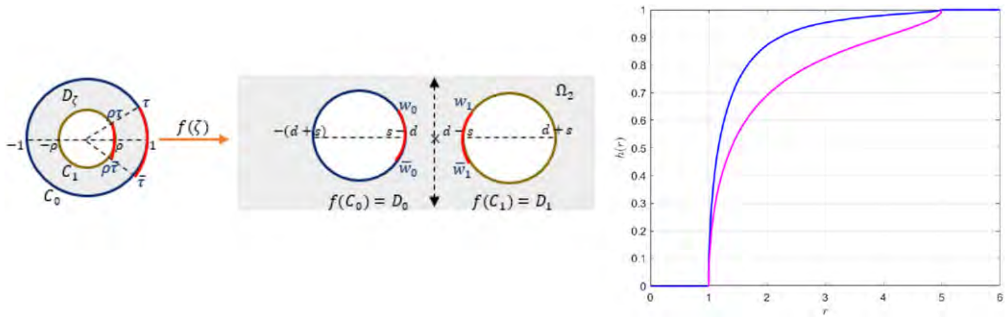

Figure 15. Conformal map from the doubly connected concentric annulus D_ζ onto domain Ω_2 with equal discs with basepoint $z_0 = 0$, for the regime $d - s \le r < d + s$ (left) and graphs of $h(r)$ for Ω_2 (blue) and for $\Omega_1 = \mathbb{C}\backslash\{|z-3| \le 2\}$ (magenta) (right). The set E_r and its preimage are shown in red.

The h-function $h_{\Omega_2,-k}(r)$ is given implicitly by $\mathrm{Im}[W_0(\zeta_0,\tau,\overline{\tau})]$, $\mathrm{Im}[W_0(\zeta_0,1,1)]$ and $\mathrm{Im}[W_1(\zeta_0,\sigma,\overline{\sigma})]$ for the second, third and fourth regimes of r, respectively, where $\tau = \mathrm{e}^{\mathrm{i}\phi}$ and $\sigma = \rho\,\mathrm{e}^{\mathrm{i}\phi}$, and where the potential functions W_0 and W_1 are as in (4.20) and (4.19), respectively.

Example 5.2 (Two equal discs with z_0 midway between them). Consider the same domain $\Omega_2 = \mathbb{C}\backslash(\{|z+d| \le s\} \cup \{|z-d| \le s\})$, with $d > s > 0$. The Möbius map f and ρ are the same as in example 5.1. This time, we fix the basepoint z_0 at the origin, midway between the boundary circles in the domain Ω_2. Then its preimage is $\zeta_0 = f^{-1}(z_0) = \sqrt{\rho}$, from equation (5.1). For the regime $d - s \le r < d + s$, the capture circle $|z - z_0| = r$ encloses an arc of equal size on each of the two boundary circles in Ω_2. See the left-hand image of figure 15. In this case, the h-function computation is similar to that in example 4.2. Here, the points w_0, $\overline{w}_0$, w_1 and $\overline{w}_1$ are the images under f of τ, $\overline{\tau}$, $\rho\tau$ and $\rho\overline{\tau}$, respectively, with $\tau = \mathrm{e}^{\mathrm{i}\phi}$ and $\sigma = \rho\,\mathrm{e}^{\mathrm{i}\psi}$ such that $\mathrm{Im}\tau > 0$ and $\mathrm{Im}\sigma > 0$.

The graph in blue in the right-hand image of figure 15 shows the h-function of the domain Ω_2 with $d = 3$ and $s = 2$, and with basepoint $z_0 = 0$. How does the h-function change when we remove the disc $\{|z+3| \le 2\}$ from the doubly connected domain $\Omega_2 = \mathbb{C}\backslash(\{|z+3| \le 2\} \cup \{|z-3| \le 2\})$, forming the simply connected domain $\Omega_1 = \mathbb{C}\backslash\{|z-3| \le 2\}$, while keeping the basepoint $z_0 = 0$ unchanged? For comparison, the graph in magenta shows the h-function of this larger domain Ω_1.

Example 5.3 (Two equal discs with z_0 off-centre between them). Again, we consider the domain $\Omega_2 = \mathbb{C}\backslash(\{|z+d| \le s\} \cup \{|z-d| \le s\})$, with $d > s > 0$, as in examples 5.1 and 5.2. Now we fix the basepoint between the discs, but off-centre, with $0 < z_0 = k < d - s$, and preimage $\zeta_0 = f^{-1}(z_0)$. The left-hand image of figure 16 illustrates the regime $k + (d - s) \le r < (d + s) - k$ for this off-centre basepoint z_0. The right-hand image of figure 16 shows the graph of the h-function of the domain Ω_2 with $z_0 = k = 0.5$, $d = 3$ and $s = 2$.

The h-function $h_{\Omega_2,k}(r)$ is given by $\mathrm{Im}[W_1(\zeta_0,\sigma,\overline{\sigma})]$, $\mathrm{Im}[W(\zeta_0,\tau,\overline{\tau},\sigma,\overline{\sigma})]$ and $\mathrm{Im}[W_0(\zeta_0,\tau,\overline{\tau})]$ for the second, third and fourth regimes of r, respectively, where $\tau = \mathrm{e}^{\mathrm{i}\psi}$ and $\sigma = \rho\,\mathrm{e}^{\mathrm{i}\phi}$, and the three potentials W_1, W and W_0 are the same as in example 4.3.

Example 5.4 (Two unequal discs with z_0 to their left). Consider the domain $\Omega_2 = \mathbb{C}\backslash(\{|z| \le 1\} \cup \{|z - 2.5| \le 0.5\})$. Fix the basepoint $z_0 = -2 \in \Omega_2$. The Möbius map

$$f(\zeta) = \frac{\zeta - \lambda}{\lambda\zeta - 1},$$

where $\lambda = (7 + 2\sqrt{6})/5$, transforms the concentric annulus $D_\zeta = \{\zeta \in \mathbb{C} : \rho < |\zeta| < 1\}$ with $\rho = 5 - 2\sqrt{6}$ onto the complement Ω_2 of the two unequal discs $|z| \le 1$ and $|z - 2.5| \le 0.5$. Let $\zeta_0 = f^{-1}(-2) \in D_\zeta$ be the preimage of the basepoint $z_0 = -2$.

For the regime $1 \le r < 3$, the capture circle covers part of the left-most boundary circle in Ω_2. See the left-hand image of figure 17. The points w_0 and $\overline{w}_0$ are the images of τ and $\overline{\tau}$, respectively.

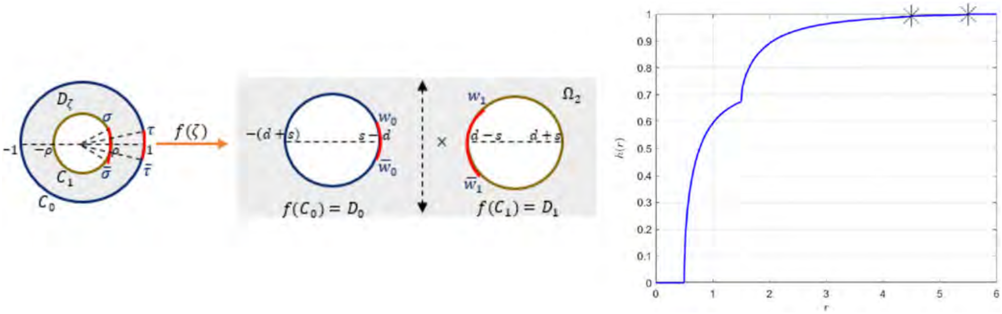

Figure 16. Conformal map from the doubly connected concentric annulus D_ζ onto domain Ω_2 with equal discs with basepoint $z_0 = k$, for the regime $k + (d - s) \le r < (d + s) - k$ (left) and graph of $h(r)$ (right). For clarity, the fourth regime in the graph of $h(r)$ is delineated by $*$ symbols. The set E_r and its preimage are shown in red.

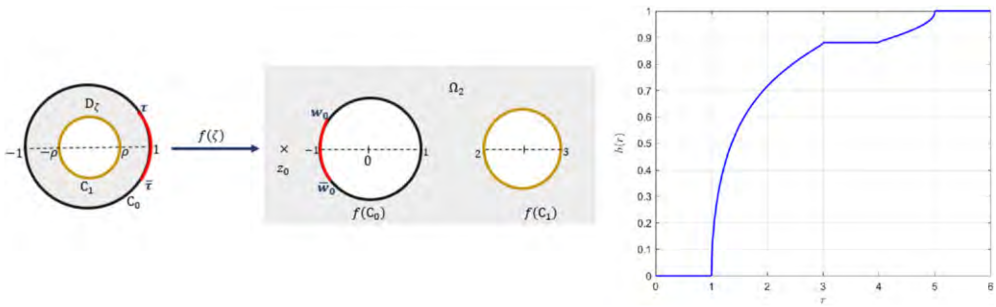

Figure 17. Conformal map from the doubly connected concentric annulus D_ζ to domain Ω_2 with unequal discs with basepoint $z_0 = -2$, for the regime $1 \le r < 3$ (left) and graph of $h(r)$ (right). The set E_r and its preimage are shown in red. The step height of $h(r)$ is $h(3) = \mathrm{Im}[W_0(\zeta_0, -1, -1)] = 0.8805$.

For this range of r, the points τ and $\overline{\tau}$ lie on the outer boundary circle of D_ζ, where $\tau = \mathrm{e}^{\mathrm{i}\phi}$ and $\mathrm{Im}\tau > 0$. The right-hand image of figure 17 shows the graph of $h(r)$ for Ω_2 with basepoint $z_0 = -2$.

The h-function $h_{\Omega_2,-2}(r)$ is given by $\mathrm{Im}[W_0(\zeta_0, \tau, \overline{\tau})]$, $\mathrm{Im}[W_0(\zeta_0, -1, -1)]$ and $\mathrm{Im}[W_1(\zeta_0, \sigma, \overline{\sigma})]$ for the second, third and fourth regimes of r, respectively, where $\tau = \mathrm{e}^{\mathrm{i}\phi}$ and $\sigma = \rho\,\mathrm{e}^{\mathrm{i}\phi}$, and

$$W_0(\zeta, \tau, \overline{\tau}) = \frac{1}{\pi}\left(\log\left[-\tau\frac{P(\zeta/\tau, \rho)}{P(\zeta/\overline{\tau}, \rho)}\right] - \mathrm{i}\phi\frac{\log\zeta}{\log\rho} + \mathrm{i}\pi\right) \tag{5.2}$$

and

$$W_1(\zeta, \sigma, \overline{\sigma}) = \frac{1}{\pi}\left(\log\left[\sigma\frac{P(\zeta/\sigma, \rho)}{P(\zeta/\overline{\sigma}, \rho)}\right] - \mathrm{i}\phi\frac{\log\zeta}{\log\rho} + \mathrm{i}(\pi + \phi)\right). \tag{5.3}$$

Example 5.5 (Two unequal discs with z_0 between them). Consider the same domain $\Omega_2 = \mathbb{C}\backslash(\{|z| \le 1\} \cup \{|z - 2.5| \le 0.5\})$ as in example 5.4, but with the basepoint $z_0 \in \mathbb{R}$ now lying between the boundary circles in Ω_2. We pick $z_0 = 1.75 \in \Omega_2$ so that $\zeta_0 = f^{-1}(1.75) \in D_\zeta$. The left-hand image of figure 18 is drawn for the third regime $0.75 \le r < 1.25$, for which the capture circle covers parts of both boundary circles in Ω_2. The right-hand image of figure 18 shows the graph of $h(r)$.

In contrast to example 5.4, as r increases through the third regime of r, the capture circle traverses a domain where it does not intersect the boundary of the target domain and so the h-function is constant, here for the third regime there is no such region and the h-function is not constant. The h-function $h_{\Omega_2,1.75}(r)$ is given by $\mathrm{Im}[W_1(\zeta_0, \sigma, \overline{\sigma})]$, $\mathrm{Im}[W(\zeta_0, \tau, \overline{\tau}, \sigma, \overline{\sigma})]$ and $\mathrm{Im}[W_0(\zeta_0, \tau, \overline{\tau})]$ for the second, third and fourth regimes of r, respectively, where $\sigma = \rho\,\mathrm{e}^{\mathrm{i}\psi}$ and

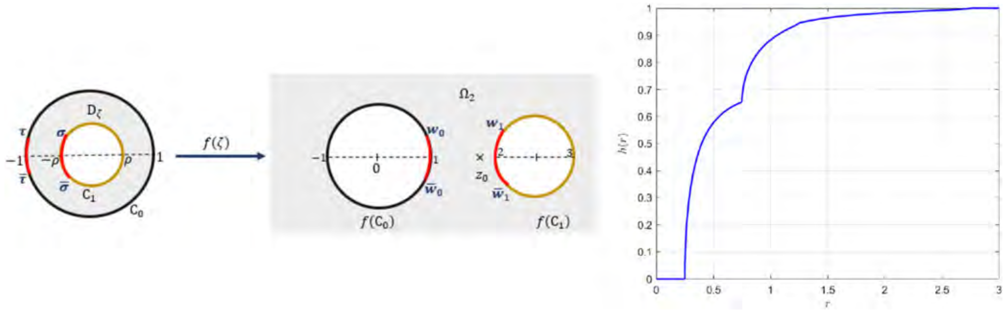

Figure 18. Conformal map from the doubly connected concentric annulus D_ζ to domain Ω_2 with unequal discs with basepoint $z_0 = 1.75$, for the regime $0.75 \leq r < 1.25$ (left) and graph of $h(r)$ (right). The set E_r and its preimage are shown in red.

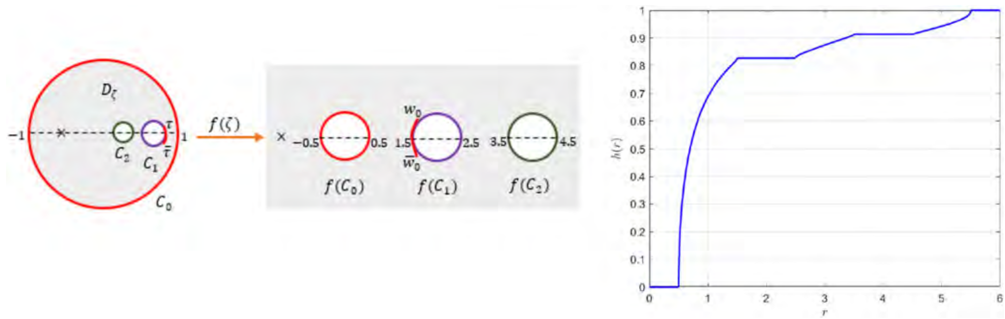

Figure 19. Conformal map from triply connected circular domain D_ζ to domain Ω_3 with equal discs with basepoint $z_0 = -1$, for the regime $2.5 \leq r < 3.5$ (left) and graph of $h(r)$ (right). The set E_r and its preimage are shown in red. The step heights of $h(r)$ are 0.8277 and 0.9138.

$\tau = e^{i\phi}$ are such that $\mathrm{Im}\sigma > 0$ and $\mathrm{Im}\tau > 0$, and

$$W_1(\zeta,\sigma,\overline{\sigma}) = \frac{1}{\pi}\left(\log\left[\sigma\frac{P(\zeta/\sigma,\rho)}{P(\zeta/\overline{\sigma},\rho)}\right] + i(\pi-\psi)\frac{\log\zeta}{\log\rho} + i\psi\right), \tag{5.4}$$

$$W(\zeta,\tau,\overline{\tau},\sigma,\overline{\sigma}) = -\frac{1}{\pi}\left(\log\left[-\frac{\tau}{\sigma^2}\frac{P(\zeta/\tau,\rho)P(\zeta/\overline{\sigma},\rho)}{P(\zeta/\overline{\tau},\rho)P(\zeta/\sigma,\rho)}\right] - i(\phi-\psi)\frac{\log\zeta}{\log\rho}\right) \tag{5.5}$$

and

$$W_0(\zeta,\tau,\overline{\tau}) = -\frac{1}{\pi}\left(\log\left[-\tau\frac{P(\zeta/\tau,\rho)}{P(\zeta/\overline{\tau},\rho)}\right] - i\phi\frac{\log\zeta}{\log\rho}\right). \tag{5.6}$$

(b) Higher connectivity case

In this final section, we discuss the h-functions for domains Ω_N given as the complement of N equal-sized discs with collinear centres, when the basepoint z_0 is fixed to one side of all the discs. We use a Möbius map $f(\zeta)$ which transforms an N-connected circular domain D_ζ onto the domain Ω_N. See figure 19.

In the domain Ω_N, the boundary circles are labelled in order from left to right as the images under f of the boundary circles $C_0, \ldots, C_{N-1}$ in D_ζ. When the basepoint z_0 is fixed to the left of all boundary circles in Ω_N, the same formulae given in §§5a and 5b of [1] hold for the h-function of Ω_N, though as usual, the dependence on r of the points τ and $\overline{\tau}$ that appear as arguments of our potential function varies with the specific form of the conformal map $f: D_\zeta \to \Omega_N$. We use these formulae for the following example 5.6, where $N = 3$.

Example 5.6 (Three equal discs with z_0 to their left). Consider the domain Ω_3 given as the complement of three equal-sized equally spaced discs of radius s, with centres lying on the real axis at 0, d and $2d$, where $d > 2s > 0$, and where the basepoint $z_0 = -k < -s$ lies on the negative real axis. We use a triply connected circular domain D_ζ whose boundaries are three circles C_0, C_1 and C_2, where the circles C_1 and C_2 are centred at δ_1 and δ_2 with radii q_1 and q_2, respectively. The conformal map $f(\zeta) = s/\zeta$ transforms the triply connected circular domain D_ζ onto the unbounded domain Ω_3. In D_ζ, as usual, C_0 is the unit circle, and we see from the form of $f(\zeta)$ that the centres and radii of C_1 and C_2 are given by

$$\delta_1 = \frac{\mathrm{d}s}{\mathrm{d}^2 - s^2}, \quad \delta_2 = \frac{2\mathrm{d}s}{4\mathrm{d}^2 - s^2}, \quad q_1 = \frac{s^2}{\mathrm{d}^2 - s^2} \quad \text{and} \quad q_2 = \frac{s^2}{4d^2 - s^2}.$$

We choose $d = 2$ and $s = 1/2$, and set the basepoint $z_0 = -1 \in \Omega_3$. The left-hand image of figure 19 shows the set E_r for the regime $2.5 \le r < 3.5$. Here, the preimages of w_0 and $\overline{w}_0$ are the points τ and $\overline{\tau}$, respectively, on ∂D_ζ. The right-hand image of figure 19 shows the graph of the h-function for the domain Ω_3 with basepoint $z_0 = -1$.

The calculation of the h-function follows the same steps as for the triply connected slit domain in §4a(iii), with the basepoint preimage $\zeta_0 = -0.5 \in D_\zeta$.

6. Conclusion

This paper has presented ways to generalize the work of Green *et al.* [1] to construct the h-functions for a variety of multiply connected domains with differing basepoint locations. We have demonstrated how to make numerous h-function calculations through the derivation of a procedure that can treat diverse geometries of domain boundary (consisting of either rectilinear slits or circles) and different locations of the basepoint. As was done in [1], we have again advocated both the usefulness and versatility of the calculus of the prime function, as well as highlighting the central role played by the various Cayley-type maps when constructing our h-function formulae. The examples presented in this paper also give solutions to instances of a variant of the CSEP.

The formulae we have presented, both for our conformal mappings and for our h-functions, are valid for any finite connectivity for a particular class of domain, and robust software based on the theory in [22] to compute the prime function was used to make the numerical computations in this paper. In principle, the formulae we have constructed in this paper can be used to make h-function calculations when the domain connectivity is very high. An alternative approach for computing h-functions for highly multiply connected slit domains, based on a fast boundary integral equation method, can be found in [14].

It is of interest to investigate whether the constructive methods presented in this paper can be employed to begin making calculations of the so-called *g-functions* of multiply connected domains; these functions are closely related to h-functions and new results for them in simply connected domains will appear in [27]. Furthermore, there will be a companion paper to this paper which again uses the theoretical framework centred around the prime function, and addresses the inverse problem concerning the recovery of circular arc domains given a particular h-function graph [28].

Data accessibility. The MATLAB codes used for numerical simulation in this paper can be found at [29].

Declaration of AI use. We have not used AI-assisted technologies in creating this article.

Authors' contributions. C.C.G.: conceptualization, formal analysis, investigation, methodology, resources, validation, visualization, writing—original draft and writing—review and editing; A.M.: conceptualization, formal analysis, investigation, methodology, resources, validation, visualization, writing—original draft and writing—review and editing; L.A.W.: conceptualization, formal analysis, investigation, methodology, resources, validation, visualization, writing—original draft and writing—review and editing.

All authors gave final approval for publication and agreed to be held accountable for the work performed therein.

Conflict of interest declaration. We declare we have no competing interests.

Funding. C.C.G. acknowledges the support of an Australian Research Council Discovery Early Career Researcher Award (ARC-DE180101098) and a LEAPS-MPS grant from the National Science Foundation (no. 2532158). A.M. acknowledges the support of an Australian Government Research Training Program Scholarship and a UniSA International HDR Fee Offset Scholarship. L.A.W. acknowledges the support of Australian Research Council Discovery grant no. ARC-DP160100153.
Acknowledgements. We thank the anonymous referees for their suggestions, which have improved this paper.

References

1. Green CC, Snipes MA, Ward LA, Crowdy DG. 2022 Harmonic-measure distribution functions for a class of multiply connected symmetrical slit domains. *Proc. R. Soc. A* **478**, 20210832. (doi:10.1098/rspa.2021.0832)
2. Kakutani S. 1944 Two-dimensional Brownian motion and harmonic functions. *Proc. Imp. Acad. Tokyo* **20**, 706–714.
3. Walden BL, Ward LA. 1996 Distributions of harmonic measure for planar domains. In *Proc. 16th Nevanlinna Colloquium, Joensuu* (eds I Laine, O Martio), *Joensuu, Finland, 1–5 August 1995*, pp. 289–299. Berlin: Walter de Gruyter.
4. Brannan DA, Hayman WK. 1989 Research problems in complex analysis. *Bull. Lond. Math. Soc.* **21**, 1–35. (doi:10.1112/blms/21.1.1)
5. Snipes MA, Ward LA. 2016 Harmonic measure distributions of planar domains: a survey. *J. Anal.* **24**, 293–330. (doi:10.1007/s41478-016-0019-0)
6. Mahenthiram A. 2022 Harmonic-measure distribution functions, and related functions, for simply connected and multiply connected two-dimensional regions. PhD thesis, Adelaide, Australia: University of South Australia.
7. Mahenthiram A. 2023 Computing *h*-functions of some planar simply connected two-dimensional regions. *Taiwan. J. Math.* **27**, 931–952. (doi:10.11650/tjm/230704)
8. Mahenthiram A. 2025 New harmonic-measure distribution functions of some simply connected planar regions in the complex plane. *Rev. Unión Mat. Argent.* (doi:10.33044/revuma.4038)
9. Mahenthiram A, Walden BL, Ward LA. In preparation. Harmonic-measure distribution functions for new planar simply connected regions, and behaviour of their derivatives.
10. Crowdy DG. 2008 Geometric function theory: a modern view of a classical subject. *Nonlinearity* **21**, T205–T219. (doi:10.1088/0951-7715/21/10/T04)
11. Crowdy DG. 2020 Solving problems in multiply connected domains. *CBMS-NSF Regional Conf. Series in Applied Mathematics*, vol. 97. Philadelphia, PA: SIAM.
12. Crowdy DG. 2007 Schwarz-Christoffel mappings to unbounded multiply connected polygonal regions. *Math. Proc. Camb. Phil. Soc.* **142**, 319–339. (doi:10.1017/S0305004106009832)
13. Mahenthiram A. 2024 Harmonic-measure distribution functions of simply connected and doubly connected polygonal domains. *J. Math. Anal. Appl.* **537**, 128308. (doi:10.1016/j.jmaa.2024.128308)
14. Green CC, Nasser MMS. 2024 Towards computing the harmonic-measure distribution function for the middle-thirds Cantor set. *J. Comput. Appl. Math.* **448**, 115903. (doi:10.1016/j.cam.2024.115903)
15. Boudabra M, Markowsky G. 2020 Remarks on Gross' technique for obtaining a conformal Skorokhod embedding of planar Brownian motion. *Electron. Commun. Probab.* **25**, 20. (doi:10.1214/20-ECP300)
16. Gross R. 2019 A conformal Skorokhod embedding. *Electron. Commun. Probab.* **24**, 68. (doi:10.1214/19-ECP272)
17. Mariano P, Panzo H. 2020 Conformal Skorokhod embeddings and related extremal problems. *Electron. Commun. Probab.* **25**, 42. (doi:10.1214/20-ECP324)
18. Obłój J. 2004 The Skorokhod embedding problem and its offspring. *Probab. Surv.* **1**, 321–390.
19. Root DH. 1969 The existence of certain stopping times on Brownian motion. *Ann. Math. Statist.* **40**, 715–718. (doi:10.1214/aoms/1177697749)
20. Skorokhod AV. 1961 *Studies in the theory of random processes* (Russian), Izdat. Kiev. Univ., Kiev. English transl. Reading, MA: Addison–Wesley, 1965.
21. Kropf EH, Nelson R. 2016 SKPrime: a numerical implementation of the Schottky–Klein prime function in MATLAB. See https://github.com/ACCA-Imperial/SKPrime.

22. Crowdy DG, Kropf EH, Green CC, Nasser MMS. 2016 The Schottky–Klein prime function: a theoretical and computational tool for applications. *IMA J. Appl. Math.* **81**, 589–628. (doi:10.1093/imamat/hxw028)
23. Hejhal DA. 1972 Theta functions, kernel functions and Abelian integrals. *Mem. Am. Math. Soc.* **129**, 1–112. (doi:10.1090/memo/0129)
24. Crowdy DG, Marshall JS. 2007 Green's functions for Laplace's equation in multiply connected domains. *IMA J. Appl. Math.* **72**, 278–301. (doi:10.1093/imamat/hxm007)
25. Crowdy DG, Marshall JS. 2006 Conformal mappings between canonical multiply connected domains. *Comput. Methods Funct. Theory* **6**, 59–76. (doi:10.1007/BF03321118)
26. Crowdy DG. 2006 Analytical solutions for uniform potential flow past multiple cylinders. *Eur. J. Mech. B Fluids* **25**, 459–470. (doi:10.1016/j.euromechflu.2005.11.005)
27. Mahenthiram A, Walden BL, Ward LA. In preparation. Stephenson's g-function for simply connected planar domains.
28. Green CC, Mahenthiram A, Ward LA. In preparation. Constructive solution of the inverse problem for harmonic-measure distribution functions that are step functions.
29. Mahenthiram A, Ward L, Green C. 2025 Simuation_codes. figshare. (doi:10.6084/m9.figshare.29583569)